Comput. Methods Appl. Mech. Engrg. 199 (2010) 471–489

Contents lists available at ScienceDirect

Comput. Methods Appl. Mech. Engrg.

journal homepage: www.elsevier.com/locate/cma

An edge-based smoothed finite element method (ES-FEM) with stabilized discrete shear gap technique for analysis of Reissner–Mindlin plates

H. Nguyen-Xuan [a,c,*], G.R. Liu [a,b], C. Thai-Hoang [d], T. Nguyen-Thoi [b,c]

[a] Singapore-MIT Alliance (SMA), E4-04-10, 4 Engineering Drive 3, Singapore 117576, Singapore
[b] Center for Advanced Computations in Engineering Science (ACES), Department of Mechanical Engineering, National University of Singapore, 9 Engineering Drive 1, Singapore 117576, Singapore
[c] Department of Mechanics, Faculty of Mathematics and Computer Science, University of Science HCM, Viet Nam
[d] EMMC Center, University of Technology HCM, Viet Nam

ARTICLE INFO

Article history:
Received 27 February 2009
Received in revised form 24 June 2009
Accepted 2 September 2009
Available online 6 September 2009

Keywords:
Plate bending
Transverse shear locking
Numerical methods
Finite element method (FEM)
Edge-based smoothed finite element method (ES-FEM)
Discrete shear gap method (DSG)
Stabilized method

ABSTRACT

An edge-based smoothed finite element method (ES-FEM) for static, free vibration and buckling analyses of Reissner–Mindlin plates using 3-node triangular elements is studied in this paper. The calculation of the system stiffness matrix is performed by using the strain smoothing technique over the smoothing domains associated with edges of elements. In order to avoid the transverse shear locking and to improve the accuracy of the present formulation, the ES-FEM is incorporated with the discrete shear gap (DSG) method together with a stabilization technique to give a so-called edge-based smoothed stabilized discrete shear gap method (ES-DSG). The numerical examples demonstrated that the present ES-DSG method is free of shear locking and achieves the high accuracy compared to the exact solutions and others existing elements in the literature.

1. Introduction

Static, free vibration and buckling analyses of plate structures play an important role in engineering practices. Such a large amount of research work on plates can be found in the literature reviews [1,2], and especially major contributions in free vibration and buckling areas by Leissa [3–6], and Liew et al. [7,8].

Owing to limitations of the analytical methods, the finite element method (FEM) becomes one of the most popular numerical approaches of analyzing plate structures. In the practical applications, lower-order Reissner–Mindlin plate elements are preferred due to its simplicity and efficiency. However, these low-order plate elements in the limit of thin plates often suffer from the shear locking phenomenon which has the root of incorrect transverse forces under bending. In order to eliminate shear locking, the selective reduced integration scheme was first proposed [9–12]. The idea of the scheme is to split the strain energy into two parts, one due to bending and one due to shear. Then, two different integration rules for the bending strain and the shear strain energy are used. For example, for the 4-node quadrilateral element, the reduced integration using a single Gauss point is utilized to compute shear strain energy while the full Gauss integration using 2×2 Gauss points is used for the bending strain energy. Unfortunately, the reduced integration often causes the instability due to rank deficiency and results in zero-energy modes. It is therefore many various improvements of formulations as well as numerical techniques have been developed to overcome the shear locking phenomenon and to increase the accuracy and stability of the solution such as mixed formulation/hybrid elements [13–23], Enhanced Assumed Strain (EAS) methods [24–28] and Assumed Natural Strain (ANS) methods [29–38]. Recently, the discrete shear gap (DSG) method [39] which avoids shear locking was proposed. The DSG is somewhat similar to the ANS methods in the terms of modifying the course of certain strains within the element, but is different in the aspect of removing of collocation points. The DSG method works for elements of different orders and shapes [39].

In the effort to further advance finite element technologies, Liu et al. have applied a strain smoothing technique [40] to formulate a cell/element-based smoothed finite element method (SFEM or CS-FEM) [41–49] for 2D solids and then CS-FEM is extended to

* Corresponding author. Address: Department of Mechanics, Faculty of Mathematics and Computer Science, University of Science HCM, Viet Nam. Tel.: +65 9860 4962.
E-mail addresses: smanxh@nus.edu.sg, nxhung@hcmuns.edu.vn (H. Nguyen-Xuan).

0045-7825/$ - see front matter © 2009 Published by Elsevier B.V.
doi:10.1016/j.cma.2009.09.001

plate and shell structures [50–52]. By using a proper number of smoothing cells in each element (for example four smoothing cells), CS-FEM can increase significantly the accuracy of the solutions [41–52]. Strain smoothing technique has recently been coupled to the extended finite element method (XFEM) [53–55] to solve fracture mechanics problems in 2D continuum and plates, e.g. [56]. A node-based smoothed finite element method (NS-FEM) [57] then has also been formulated to give upper bound solutions in the strain energy and applied to adaptive analysis [58]. Then by combining NS-FEM and FEM with a scale factor $\alpha \in [0,1]$, a new method named as the alpha finite element method (αFEM) [59] is proposed to obtain nearly exact solutions in strain energy using triangular and tetrahedral elements.

Recently, Liu et al. [60] have proposed an edge-based smoothed finite element method (ES-FEM) for static, free and forced vibration analyses of solid 2D mechanics problems. Intensive numerical results demonstrated that ES-FEM [60] possesses the following excellent properties: (1) ES-FEM model are often found super-convergent and even more accurate than those of the FEM using quadrilateral elements (FEM-Q4) with the same sets of nodes; (2) there are no spurious non-zeros energy modes found and hence the method is also temporally stable and works well for vibration analysis and (3) the implementation of the method is straightforward and no penalty parameter is used, and the computational efficiency is better than the FEM using the same sets of nodes. The ES-FEM has also been further developed to analyze piezoelectric structures [61] and 2D elastoviscoplastic problems [62]. Further more, the idea of ES-FEM has been extended for the 3D problems using tetrahedral elements to give a so-called the face-based smoothed finite element method (FS-FEM) [63].

This paper further extends ES-FEM to static, free vibration and buckling analyses of Reissner–Mindlin plates using only 3-node triangular meshes which are easily generated for the complicated domains. The calculation of the system stiffness matrix is performed using strain smoothing technique over the smoothing cells associated with edges of elements. In order to avoid transverse shear locking and to improve the accuracy of the present formulation, the ES-FEM is incorporated with the discrete shear gap (DSG) method [39] together with a stabilization technique [64] to give a so-called edge-based smoothed stabilized discrete shear gap method (ES-DSG). The numerical examples show that the present method is free of shear locking and is a strong competitor to others existing elements in the literature.

2. Governing equations and weak form

We consider a domain $\Omega \subset R^2$ occupied by reference middle surface of plate. Let w and $\boldsymbol{\beta}^T = (\beta_x, \beta_y)$ be the transverse displacement and the rotations about the y and x axes, see Fig. 1, respectively. Then the vector of three independent field variables for Mindlin plates is

$$\mathbf{u}^T = \begin{bmatrix} w & \beta_x & \beta_y \end{bmatrix}. \tag{1}$$

Let us assume that the material is homogeneous and isotropic with Young's modulus E and Poisson's ratio v. The governing differential equations of the static Mindlin–Reissner plate are

$$\begin{aligned} &\nabla \cdot \mathbf{D}^b \boldsymbol{\kappa}(\boldsymbol{\beta}) + kt\boldsymbol{\gamma} = \mathbf{0} \quad \text{in } \Omega, \\ &kt\nabla \cdot \boldsymbol{\gamma} + p = 0 \quad \text{in } \Omega, \\ &w = \bar{w}, \quad \boldsymbol{\beta} = \bar{\boldsymbol{\beta}} \quad \text{on } \Gamma = \partial\Omega, \end{aligned} \tag{2}$$

where t is the plate thickness, $p = p(x,y)$ is a distributed load per an area unit, $k = \mu E/2(1+v)$, $\mu = 5/6$ is the shear correction factor, $\mathbf{D}^b$ is the tensor of bending modulus, $\boldsymbol{\kappa}$ and $\boldsymbol{\gamma}$ are the bending and shear strains, respectively, defined by

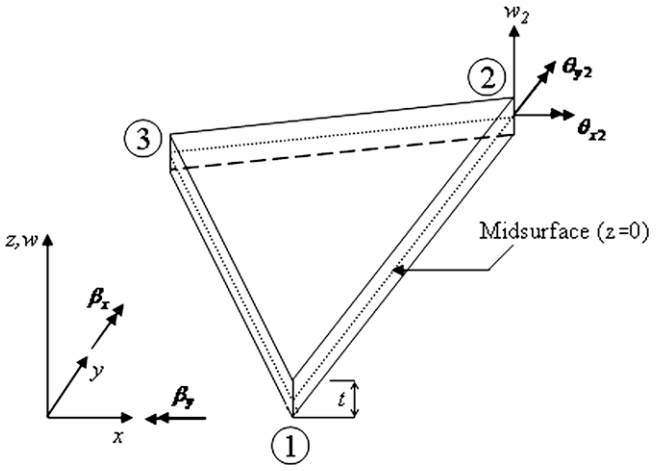

Fig. 1. 3-Node triangular element.

$$\boldsymbol{\kappa} = \mathbf{L}_d \boldsymbol{\beta}, \quad \boldsymbol{\gamma} = \nabla w + \boldsymbol{\beta}, \tag{3}$$

where $\nabla = (\partial/\partial x, \partial/\partial y)$ is the gradient vector and L_d is a differential operator matrix defined by

$$\mathbf{L}_d^T = \begin{bmatrix} \frac{\partial}{\partial x} & 0 & \frac{\partial}{\partial y} \\ 0 & \frac{\partial}{\partial y} & \frac{\partial}{\partial x} \end{bmatrix}. \tag{4}$$

The weak form of the static equilibrium equations in (2) is

$$\int_\Omega \delta\boldsymbol{\kappa}^T \mathbf{D}^b \boldsymbol{\kappa}\, d\Omega + \int_\Omega \delta\boldsymbol{\gamma}^T \mathbf{D}^s \boldsymbol{\gamma}\, d\Omega = \int_\Omega \delta w p\, d\Omega, \tag{5}$$

where $\mathbf{D}^b$ and $\mathbf{D}^s$ are the material matrices related to the bending and shear parts defined by

$$\mathbf{D}^b = \frac{Et^3}{12(1-v^2)} \begin{bmatrix} 1 & v & 0 \\ v & 1 & 0 \\ 0 & 0 & (1-v)/2 \end{bmatrix}, \quad \mathbf{D}^s = kt \begin{bmatrix} 1 & 0 \\ 0 & 1 \end{bmatrix}. \tag{6}$$

For the free vibration analysis of a Mindlin/Reissner plate model, a weak form may be derived form the dynamic form of energy principle under the assumption of the first order shear-deformation plate theory [8]:

$$\int_\Omega \delta\boldsymbol{\kappa}^T \mathbf{D}^b \boldsymbol{\kappa}\, d\Omega + \int_\Omega \delta\boldsymbol{\gamma}^T \mathbf{D}^s \boldsymbol{\gamma}\, d\Omega + \int_\Omega \delta\mathbf{u}^T \mathbf{m}\ddot{\mathbf{u}}\, d\Omega = 0, \tag{7}$$

where $\delta\mathbf{u}$ is the variation of displacement field $\mathbf{u}$, and $\mathbf{m}$ is the matrix containing the mass density ρ and thickness t

$$\mathbf{m} = \rho \begin{bmatrix} t & 0 & 0 \\ 0 & \frac{t^3}{12} & 0 \\ 0 & 0 & \frac{t^3}{12} \end{bmatrix}. \tag{8}$$

For the buckling analysis, there appears nonlinear strain under in-plane pre-buckling stresses $\hat{\boldsymbol{\sigma}}_0$. The weak form can be reformulated as [8]

$$\begin{aligned} &\int_\Omega \delta\boldsymbol{\kappa}^T \mathbf{D}^b \boldsymbol{\kappa}\, d\Omega + \int_\Omega \delta\boldsymbol{\gamma}^T \mathbf{D}^s \boldsymbol{\gamma}\, d\Omega + t\int_\Omega \nabla^T \delta w \hat{\boldsymbol{\sigma}}_0 \nabla w\, d\Omega \\ &+ \frac{t^3}{12}\int_\Omega \begin{bmatrix} \nabla^T\delta\beta_x & \nabla^T\delta\beta_y \end{bmatrix} \begin{bmatrix} \hat{\boldsymbol{\sigma}}_0 & 0 \\ 0 & \hat{\boldsymbol{\sigma}}_0 \end{bmatrix} \begin{bmatrix} \nabla\beta_x \\ \nabla\beta_y \end{bmatrix} d\Omega = 0. \end{aligned} \tag{9}$$

Eq. (9) can be rewritten as

$$\int_\Omega \delta\boldsymbol{\kappa}^T \mathbf{D}^b \boldsymbol{\kappa}\, d\Omega + \int_\Omega \delta\boldsymbol{\gamma}^T \mathbf{D}^s \boldsymbol{\gamma}\, d\Omega + \int_\Omega (\delta\boldsymbol{\varepsilon}^g)^T \boldsymbol{\tau}\ \boldsymbol{\varepsilon}^g\, d\Omega = 0, \tag{10}$$

where

$$\hat{\boldsymbol{\sigma}}_0 = \begin{bmatrix} \sigma_x^0 & \sigma_{xy}^0 \\ \sigma_{xy}^0 & \sigma_y^0 \end{bmatrix}, \quad \boldsymbol{\tau} = \begin{bmatrix} t\hat{\boldsymbol{\sigma}}_0 & 0 & 0 \\ 0 & \frac{t^3}{12}\hat{\boldsymbol{\sigma}}_0 & 0 \\ 0 & 0 & \frac{t^3}{12}\hat{\boldsymbol{\sigma}}_0 \end{bmatrix},$$

$$\boldsymbol{\varepsilon}^g = \begin{bmatrix} w_{,x} & 0 & 0 \\ w_{,y} & 0 & 0 \\ 0 & \beta_{x,x} & 0 \\ 0 & \beta_{x,y} & 0 \\ 0 & 0 & \beta_{y,x} \\ 0 & 0 & \beta_{y,y} \end{bmatrix}. \tag{11}$$

3. FEM formulation for the Reissner–Mindlin plate

Now, discretize the bounded domain Ω into N_e finite elements such that $\Omega = \bigcup_{e=1}^{N_e} \Omega^e$ and $\Omega^i \cap \Omega^j = \emptyset$, $i \neq j$. The finite element solution $\mathbf{u}^h = (w^h, \beta_x^h, \beta_y^h)^T$ of a displacement model for the Mindlin–Reissner plate is then expressed as:

$$\mathbf{u}^h = \sum_{I=1}^{N_n} \begin{bmatrix} N_I(\mathbf{x}) & 0 & 0 \\ 0 & N_I(\mathbf{x}) & 0 \\ 0 & 0 & N_I(\mathbf{x}) \end{bmatrix} \mathbf{d}_I, \tag{12}$$

where N_n is the total number of nodes, $N_I(x)$, $\mathbf{d}_I = [w_I\ \beta_{xI}\ \beta_{yI}]^T$ are shape function and the nodal degrees of freedom of $\mathbf{u}^h$ associated to node I, respectively.

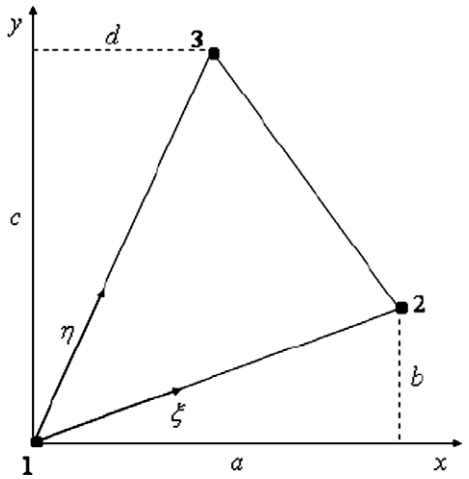

Fig. 2. 3-Node triangular element and local coordinates.

The bending, shear strains and geometrical strains can be then expressed as:

$$\boldsymbol{\kappa} = \sum_I \mathbf{B}_I^b \mathbf{d}_I, \quad \boldsymbol{\gamma}^s = \sum_I \mathbf{B}_I^s \mathbf{d}_I, \quad \boldsymbol{\varepsilon}^g = \sum_I \mathbf{B}_I^g \mathbf{d}_I, \tag{13}$$

where

$$\mathbf{B}_I^b = \begin{bmatrix} 0 & N_{I,x} & 0 \\ 0 & 0 & N_{I,y} \\ 0 & N_{I,y} & N_{I,x} \end{bmatrix}, \quad \mathbf{B}_i^s = \begin{bmatrix} N_{I,x} & N_I & 0 \\ N_{I,y} & 0 & N_I \end{bmatrix},$$

$$\mathbf{B}_I^g = \begin{bmatrix} N_{I,x} & 0 & 0 \\ N_{I,y} & 0 & 0 \\ 0 & N_{I,x} & 0 \\ 0 & N_{I,y} & 0 \\ 0 & 0 & N_{I,x} \\ 0 & 0 & N_{I,y} \end{bmatrix}. \tag{14}$$

The discretized system of equations of the Mindlin/Reissner plate using the FEM for static analysis then can be expressed as,

$$\mathbf{K}\mathbf{d} = \mathbf{F}, \tag{15}$$

where

$$K = \int_\Omega \left(\mathbf{B}^b\right)^T \mathbf{D}^b \mathbf{B}^b \, d\Omega + \int_\Omega (\mathbf{B}^s)^T \mathbf{D}^s \mathbf{B}^s \, d\Omega \tag{16}$$

is the global stiffness matrix, and the load vector

$$\mathbf{F} = \int_\Omega p\mathbf{N} \, d\Omega + \mathbf{f}^b \tag{17}$$

in which $\mathbf{f}^b$ is the remaining part of $\mathbf{F}$ subjected to prescribed boundary loads

For free vibration, we have

$$(\mathbf{K} - \omega^2 \mathbf{M})\mathbf{d} = 0, \tag{18}$$

where ω is the natural frequency, $\mathbf{M}$ is the global mass matrix

$$\mathbf{M} = \int_\Omega \mathbf{N}^T \mathbf{m} \mathbf{N} \, d\Omega. \tag{19}$$

For the buckling analysis, we have

$$(\mathbf{K} - \lambda_{cr}\mathbf{K}_g)\mathbf{d} = 0, \tag{20}$$

where

$$\mathbf{K}_g = \int_\Omega (\mathbf{B}^g)^T \boldsymbol{\tau} \mathbf{B}^g \, d\Omega \tag{21}$$

is the geometrical stiffness matrix, and λ_{cr} is the critical buckling load.

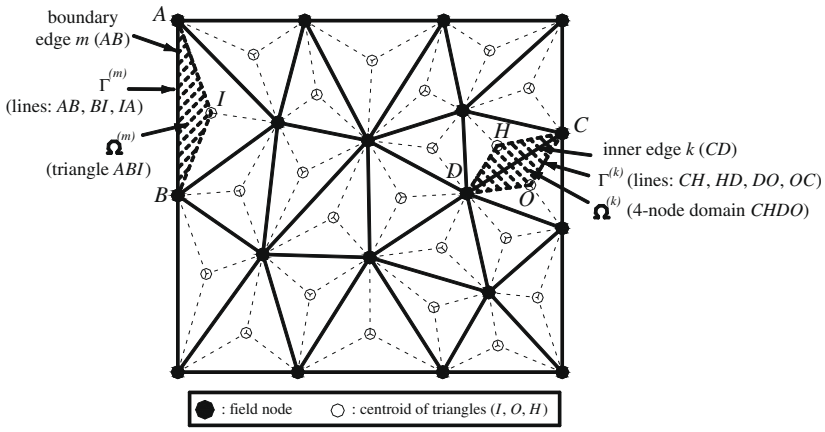

Fig. 3. Division of domain into triangular element and smoothing cells $\Omega^{(k)}$ connected to edge k of triangular elements.

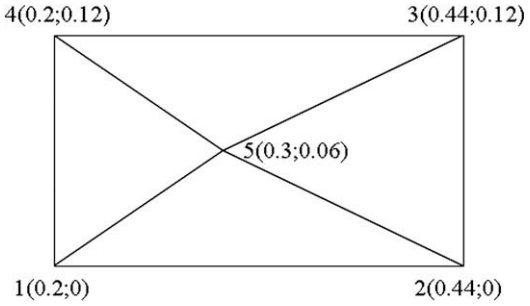

Fig. 4. Patch test of the element.

Table 1
Patch test.

Element	w_5	θ_{x5}	θ_{y5}	m_{x5}	m_{y5}	m_{xy5}
MIN3	0.6422	1.1300	−0.6400	−0.0111	−0.0111	−0.0033
DSG3	0.6422	1.1300	−0.6400	−0.0111	−0.0111	−0.0033
ES-DSG3	0.6422	1.1300	−0.6400	−0.0111	−0.0111	−0.0033
Exact	0.6422	1.1300	−0.6400	−0.0111	−0.0111	−0.0033

Now, next section aims to establish a new triangular element named an edge-based smoothed triangular element with the stabilized discrete shear gap technique (ES-DSG3) for Reissner–Mindlin plate that is a combination from:

- The ES-FEM [60] for 2D solid mechanics was found to be one of the "most" accurate models using triangular elements,
- The discrete shear gap (DSG) technique works well for shear-locking-free triangular elements based on the Reissner–Mindlin plate theory [39],
- The stabilization technique [64] helps further to improve the stability and accuracy.

The formulated ES-DSG3 will be stable and works well for both thin and thick plates using only triangular elements.

4. A formulation of ES-FEM with stabilized discrete shear technique

4.1. Brief on the DSG3 formulation

The approximation $\mathbf{u}^h = [w^h \ \beta_x^h \ \beta_y^h]^T$ of 3-node triangular element as shown in Fig. 2 for the Mindlin–Reissner plate can be written as

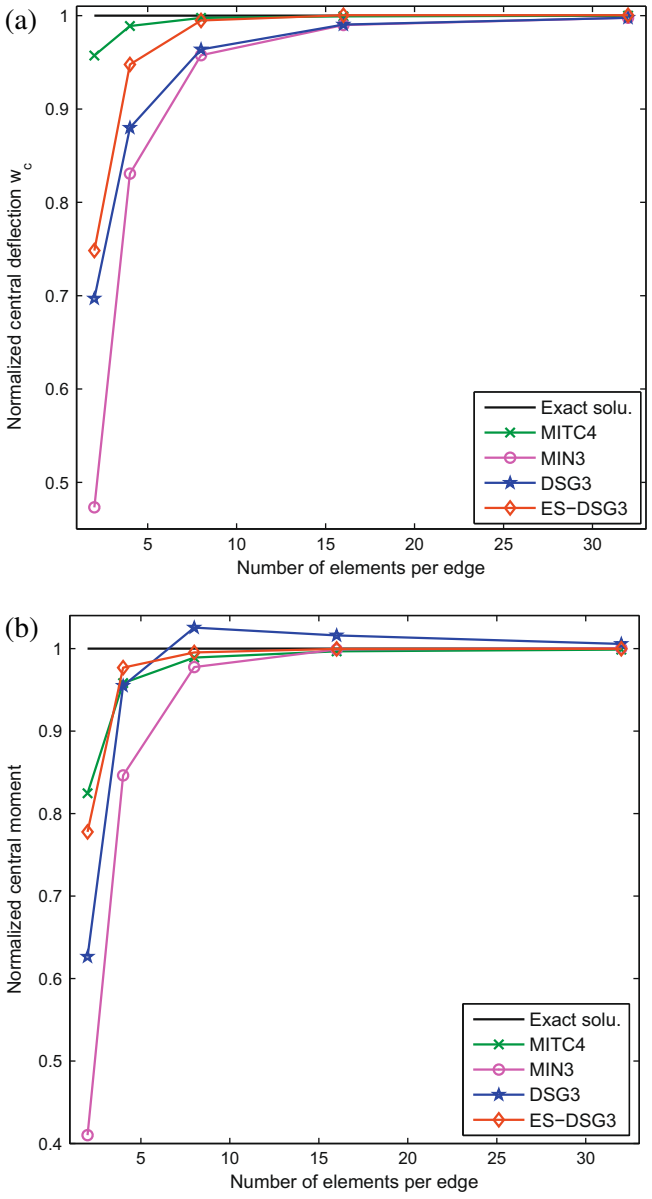

Fig. 6. Clamped plate: (a) central deflection; (b) central moment ($t/L = 0.001$).

$$\mathbf{u}^h = \sum_{I=1}^{3} \begin{bmatrix} N_I(\mathbf{x}) & 0 & 0 \\ 0 & N_I(\mathbf{x}) & 0 \\ 0 & 0 & N_I(\mathbf{x}) \end{bmatrix} \mathbf{d}_I^e, \tag{22}$$

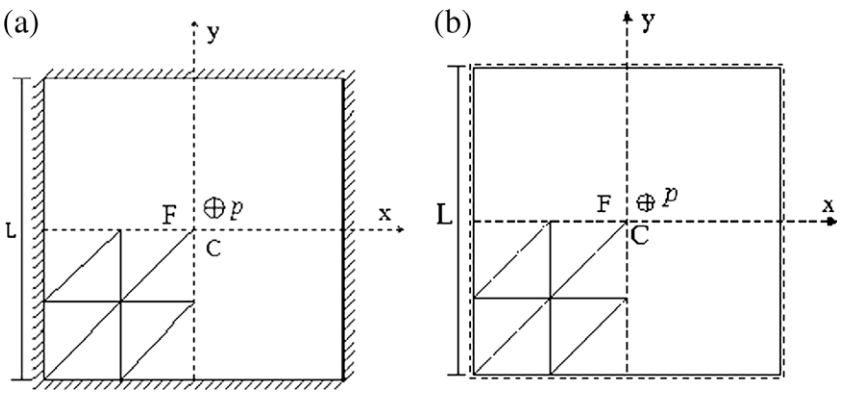

Fig. 5. Square plate model; (a) full clamped plate; (b) simply supported plate.

where $\mathbf{d}_I^e = [w_I\ \beta_{xI}\ \beta_{yI}]^T$ are the nodal degrees of freedom of $\mathbf{u}^h$ associated to node I and $N_I(x)$ is linearly shape functions defined by

$$N_1 = 1 - \xi - \eta, \quad N_2 = \xi, \quad N_3 = \eta. \tag{23}$$

The curvatures are then obtained by

$$\boldsymbol{\kappa}^h = \mathbf{B}^b \mathbf{d}^e, \tag{24}$$

where $\mathbf{d}^e$ is the nodal displacement vector of element, $\mathbf{B}^b$ contains the derivatives of the shape functions that are only constant

$$\mathbf{B}^b = \frac{1}{2A^e}\begin{bmatrix} 0 & b-c & 0 & 0 & c & 0 & 0 & -b & 0 \\ 0 & 0 & d-a & 0 & 0 & -d & 0 & 0 & a \\ 0 & d-a & b-c & 0 & -d & c & 0 & a & -b \end{bmatrix} \tag{25}$$

with $a = x_2 - x_1$, $b = y_2 - y_1$, $c = y_3 - y_1$, $d = x_3 - x_1$ and A^e is the area of the triangular element.

The geometrical strains are written as:

$$\boldsymbol{\varepsilon}^g = \mathbf{B}^g \mathbf{d}^e, \tag{26}$$

where

$$\mathbf{B}^g = \frac{1}{2A^e}\begin{bmatrix} b-c & 0 & 0 & c & 0 & 0 & -b & 0 & 0 \\ d-a & 0 & 0 & -d & 0 & 0 & a & 0 & 0 \\ 0 & b-c & 0 & 0 & c & 0 & 0 & -b & 0 \\ 0 & d-a & 0 & 0 & -d & 0 & 0 & a & 0 \\ 0 & 0 & b-c & 0 & 0 & c & 0 & 0 & -b \\ 0 & 0 & d-a & 0 & 0 & -d & 0 & 0 & a \end{bmatrix}. \tag{27}$$

As known in many literatures about Reissner–Mindlin elements, the shear locking often appears when the thickness plate becomes small. This is because the transverse shear strains do not vanish under pure bending conditions. In order to avoid this shortcoming, Bletzinger et al. [39] have proposed the discrete shear gap method (DSG) for approximating the shear strains. Results of the shear strains are briefed as

$$\boldsymbol{\gamma}^h = \mathbf{B}^s \mathbf{d}^e, \tag{28}$$

where

$$\mathbf{B}^s = \frac{1}{2A^e}\begin{bmatrix} b-c & A^e & 0 & c & \frac{ac}{2} & \frac{bc}{2} & -b & -\frac{bd}{2} & -\frac{bc}{2} \\ d-a & 0 & A^e & -d & -\frac{ad}{2} & -\frac{bd}{2} & a & \frac{ad}{2} & \frac{ac}{2} \end{bmatrix}. \tag{29}$$

Substituting Eqs. (25) and (29) into (16) and Eq. (27) into (21), the global stiffness matrices are now modified as

$$\mathbf{K}^{\mathrm{DSG3}} = \sum_{e=1}^{N_e} \mathbf{K}^{\mathrm{eDSG3}}, \tag{30}$$

$$\mathbf{K}_g^{\mathrm{DSG3}} = \sum_{e=1}^{N_e} \mathbf{K}_g^{\mathrm{eDSG3}}, \tag{31}$$

where the element stiffness matrix, $\mathbf{K}^{\mathrm{eDSG3}}$ and the element geometrical stiffness matrix, $\mathbf{K}_g^{\mathrm{eDSG3}}$, of the DSG3 element are given as

$$\begin{aligned} \mathbf{K}^{\mathrm{eDSG3}} &= \int_{\Omega^e} (\mathbf{B}^b)^T \mathbf{D}^b \mathbf{B}^b \, d\Omega + \int_{\Omega^e} (\mathbf{B}^s)^T \mathbf{D}^s \mathbf{B}^s \, d\Omega \\ &= (\mathbf{B}^b)^T \mathbf{D}^b \mathbf{B}^b A^e + (\mathbf{B}^s)^T \mathbf{D}^s \mathbf{B}^s A^e, \end{aligned} \tag{32}$$

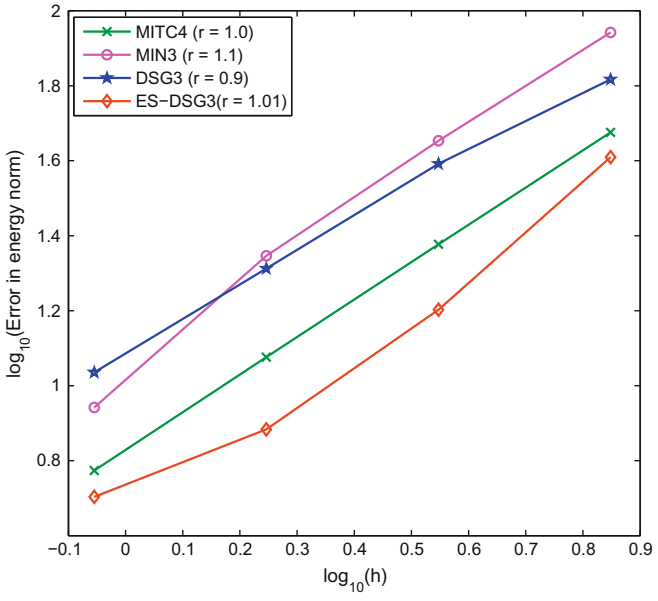

Fig. 7. The convergence rate in strain energy of a clamped plate.

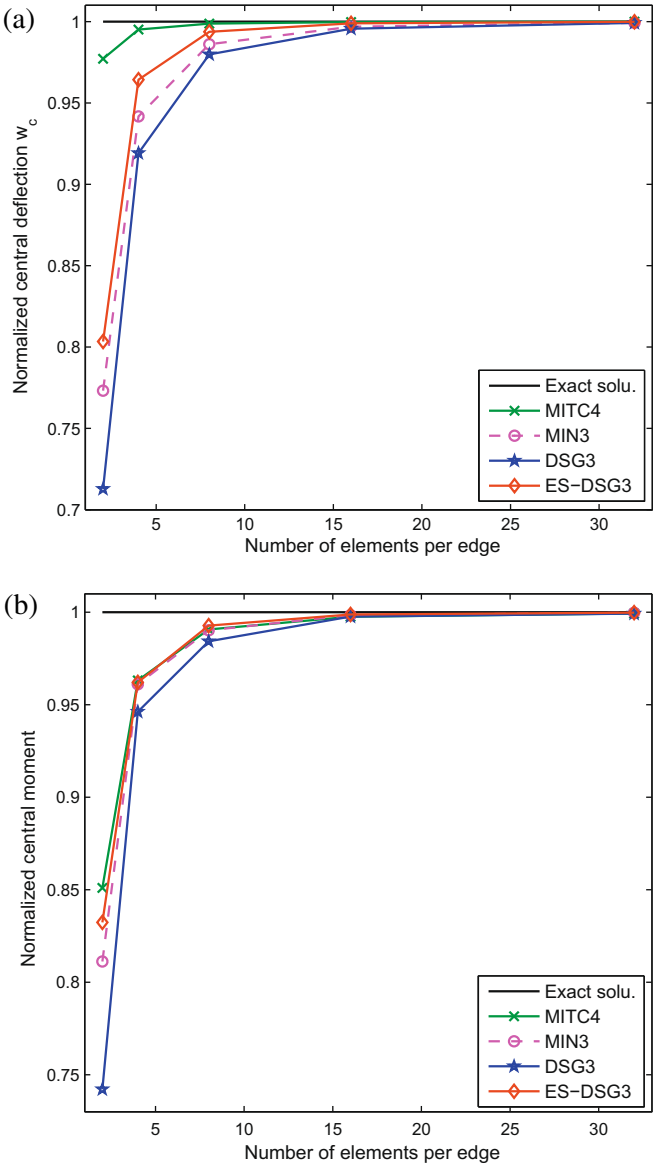

Fig. 8. Simply supported plate: (a) central deflection; (b) central moment ($t/L = 0.01$).

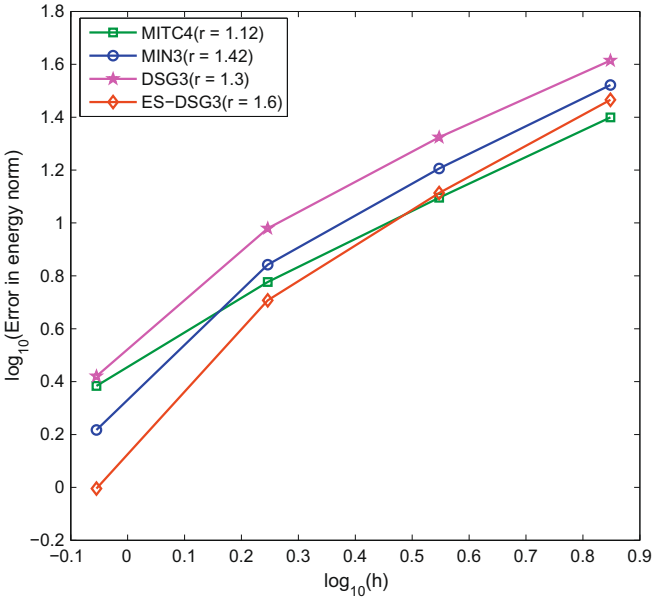

Fig. 9. The convergence rate in energy norm of a simply supported plate.

$$\mathbf{K}_g^{eDSG3} = \int_{\Omega^e} \mathbf{B}^{gT}\tau\mathbf{B}^g\,d\Omega = \mathbf{B}^{gT}\tau\mathbf{B}^g A^e. \tag{33}$$

It was mentioned that a stabilization technique [64] needs to be added to the original DSG3 element to improve significantly the accuracy of approximate solutions and to stabilize shear force oscillations presenting in the triangular element. More details for the stabilized issue of the original DSG3 element can be found in Bischoff and Bletzinger [65].[1] For this remedy, the element stiffness matrix can be modified as

$$\begin{aligned}\mathbf{K}^{\text{eDSG3}} &= \int_{\Omega^e} (\mathbf{B}^b)^T\mathbf{D}^b\mathbf{B}^b\,d\Omega + \int_{\Omega^e} (\mathbf{B}^s)^T\bar{\mathbf{D}}^s\mathbf{B}^s\,d\Omega \\ &= (\mathbf{B}^b)^T\mathbf{D}^b\mathbf{B}^b A^e + (\mathbf{B}^s)^T\bar{\mathbf{D}}^s\mathbf{B}^s A^e,\end{aligned} \tag{34}$$

where

$$\bar{\mathbf{D}}^s = \frac{kt^3}{t^2+\alpha h_e^2}\begin{bmatrix}1 & 0\\ 0 & 1\end{bmatrix}, \tag{35}$$

where h_e is the longest length of the edges of the element and α is a positive constant [64].

4.2. Formulation of ES-DSG3

In the ES-FEM, we do not use the compatible strain fields as in (13) but "smoothed" strains over local smoothing domains associated with the edges of elements. Naturally the integration for the stiffness matrix and the geometrical stiffness matrix is no longer based on elements, but on these smoothing domains. These local smoothing domains are constructed based on edges of the elements such that $\Omega = \bigcup_{k=1}^{N_{ed}} \Omega^{(k)}$ and $\Omega^{(i)} \cap \Omega^{(j)} = \emptyset$ for $i \neq j$, in which N_{ed} is the total number of edges of all elements in the entire problem domain. For triangular elements, the smoothing domain $\Omega^{(k)}$ associated with the edge k is created by connecting two end-nodes of the edge to centroids of adjacent elements as shown in Fig. 3.

[1] The DSG3 was initially labeled in the original contribution [39] without any stabilization. The SDSG3 [65] was then named due to combining the stabilized technique [64]. For abbreviation, the DSG3 still is used in this paper, but with the stabilization.

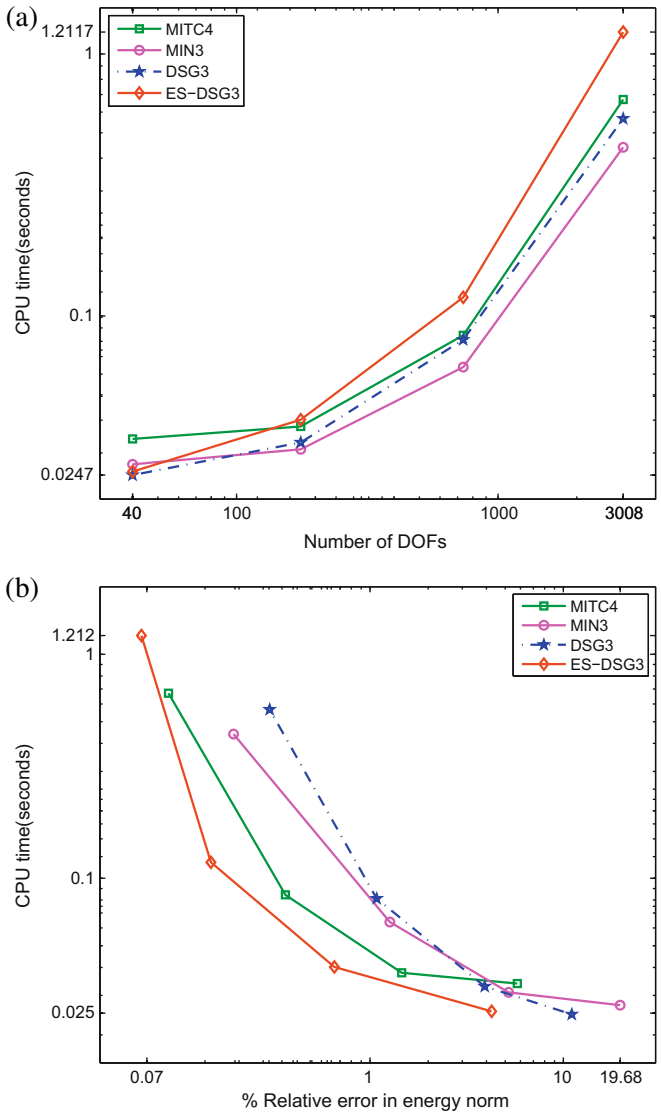

Fig. 10. The illustration of computational cost for clamped plate: (a) CPU times versus DOFs; (b) comparison of the efficiency of computation time in terms of energy error norm.

Introducing average curvature, shear strain and geometrical strain over the cell $\Omega^{(k)}$ defined by

$$\begin{aligned}\tilde{\boldsymbol{\kappa}}_k &= \frac{1}{A^{(k)}}\int_{\Omega^{(k)}} \boldsymbol{\kappa}(\mathbf{x})\,d\Omega, \quad \tilde{\gamma}_k = \frac{1}{A^{(k)}}\int_{\Omega^{(k)}} \gamma(\mathbf{x})\,d\Omega, \\ \tilde{\boldsymbol{\varepsilon}}_k^g &= \frac{1}{A^{(k)}}\int_{\Omega^{(k)}} \boldsymbol{\varepsilon}^g(\mathbf{x})\,d\Omega,\end{aligned} \tag{36}$$

where $A^{(k)}$ is the area of the smoothing cell $\Omega^{(k)}$ and is computed by

$$A^{(k)} = \int_{\Omega^{(k)}} d\Omega = \frac{1}{3}\sum_{i=1}^{N_e^k} A_i \tag{37}$$

where N_e^k is the number of elements attached to the edge k ($N_e^k = 1$ for the boundary edges and $N_e^k = 2$ for inner edges as shown in Fig. 3) and A_i is the area of the ith element attached to the edge k.

Substituting Eqs. (24), (28) and (26) into Eq. (36), the average strains at edge k can be expressed in the following form

$$\tilde{\boldsymbol{\kappa}}_k = \sum_{I=1}^{N_n^k} \tilde{\mathbf{B}}_I^b(\mathbf{x}_k)\mathbf{d}_I, \quad \tilde{\gamma}_k = \sum_{I=1}^{N_n^k} \tilde{\mathbf{B}}_I^s(\mathbf{x}_k)\mathbf{d}_I, \quad \tilde{\boldsymbol{\varepsilon}}_k^g = \sum_{I=1}^{N_n^k} \tilde{\mathbf{B}}_I^g(\mathbf{x}_k)\mathbf{d}_I, \tag{38}$$

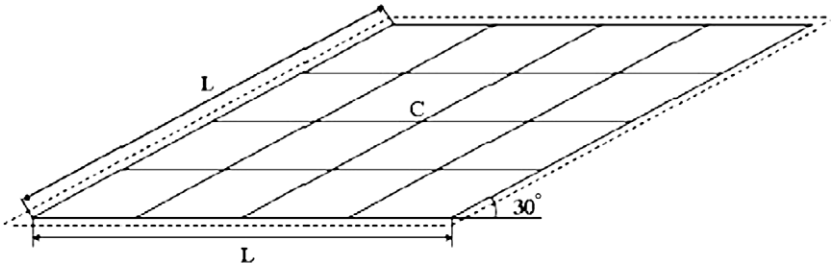

Fig. 11. A simply supported skew Morley's model.

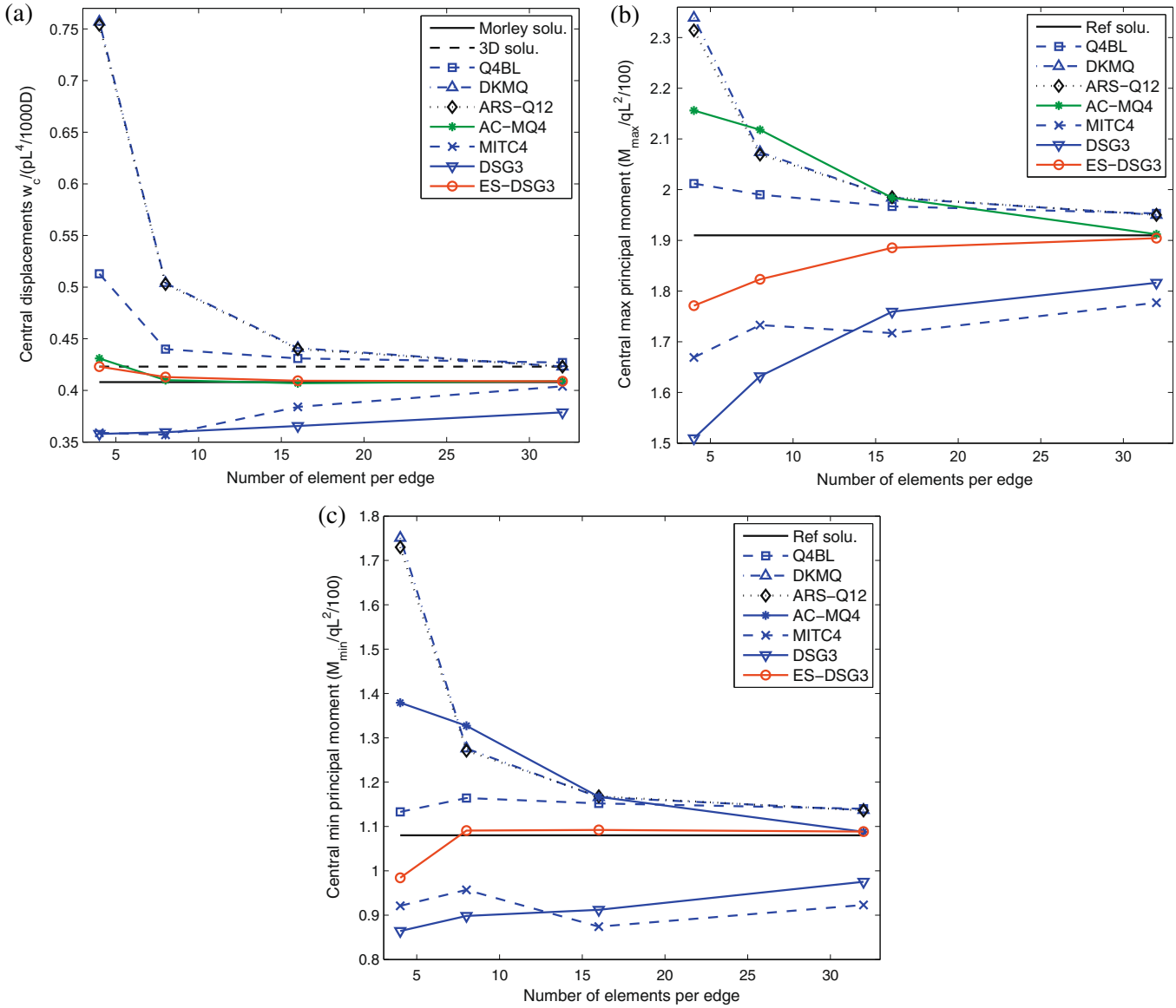

Fig. 12. Morley plates: (a) central deflection; (b) central max principle moment; (c) central min principle moment.

where N_n^k is the number of nodes belonging to elements directly connected to edge k ($N_n^k = 3$ for boundary edges and $N_n^k = 4$ for inner edges as shown in Fig. 3) and $\tilde{\mathbf{B}}_I^b(\mathbf{x}_k), \tilde{\mathbf{B}}_I^s(\mathbf{x}_k)$ and $\tilde{\mathbf{B}}_I^g(\mathbf{x}_k)$ are the average gradient matrices corresponding to the smoothing cell $\Omega^{(k)}$ and given by

$$\tilde{\mathbf{B}}_I^b(\mathbf{x}_k) = \frac{1}{A^{(k)}} \sum_{i=1}^{N_e^k} \frac{1}{3} A_i \mathbf{B}_i^b, \quad \tilde{\mathbf{B}}_I^s(\mathbf{x}_k) = \frac{1}{A^{(k)}} \sum_{i=1}^{N_e^k} \frac{1}{3} A_i \mathbf{B}_i^s,$$
$$\tilde{\mathbf{B}}_I^g(\mathbf{x}_k) = \frac{1}{A^{(k)}} \sum_{i=1}^{N_e^k} \frac{1}{3} A_i \mathbf{B}_i^g, \tag{39}$$

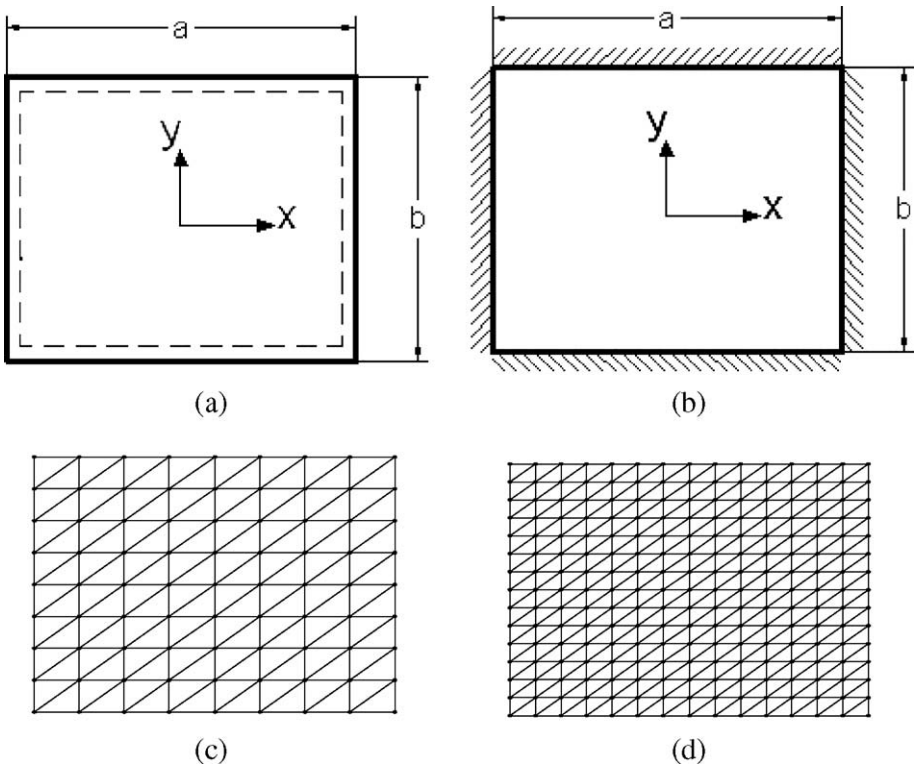

Fig. 13. Plates and initial mesh: (a) supported plate (b) clamped plate and (c,d) triangular meshes.

Table 2
A non-dimensional frequency parameter ϖ of a SSSS plate ($a/b = 1$).

t/a	Elements	Mode sequence number					
		1	2	3	4	5	6
0.005	DSG3	5.5626	8.8148	11.8281	13.4126	18.1948	19.2897
		4.7327	7.4926	8.2237	10.2755	11.6968	12.4915
		4.5131	7.1502	7.3169	9.3628	10.3772	10.4461
		4.4781	7.0905	7.1718	9.1455	10.1643	10.1814
	ES-DSG3	4.9168	8.1996	9.4593	11.5035	14.2016	15.0164
		4.5376	7.2981	7.4659	9.6486	10.8937	11.0280
		4.4641	7.0870	7.1193	9.0582	10.1444	10.1489
		4.4537	7.0565	7.0729	8.9731	10.0410	10.0422
	Exact [68]	4.443	7.025	7.025	8.886	9.935	9.935
0.1	DSG3	4.9970	8.1490	9.4311	11.3540	14.1290	14.9353
		4.4891	7.0697	7.2530	9.1263	10.2195	10.3361
		4.3943	6.8227	6.8587	8.5447	9.4557	9.4616
		4.3809	6.7854	6.8037	8.4543	9.3441	9.3457
	ES-DSG3	4.7376	7.6580	8.4524	10.1882	12.1227	12.7533
		4.4433	6.9495	7.0727	8.8487	9.8575	9.9221
		4.3846	6.7922	6.8196	8.4744	9.3666	9.3698
		4.3759	6.7692	6.7834	8.4173	9.2968	9.2976
	Exact [68]	4.37	6.74	6.74	8.35	9.22	9.22

where $\mathbf{B}_i^b$ (of 3×3 matrix), $\mathbf{B}_i^s$ (of 2×3 matrix) and $\mathbf{B}_i^g$ (of 6×3 matrix) are obtained from matrices in (25), (29), and (27), respectively.

Therefore the global stiffness and geometrical stiffness matrices of the ES-DSG3 element are assembled by

$$\tilde{\mathbf{K}} = \sum_{k=1}^{N_{ed}} \tilde{\mathbf{K}}^{(k)}, \tag{40}$$

$$\tilde{\mathbf{K}}_g = \sum_{k=1}^{N_{ed}} \tilde{\mathbf{K}}_g^{(k)}, \tag{41}$$

where the edge stiffness, $\tilde{\mathbf{K}}^{(k)}$, and geometrical stiffness, $\tilde{\mathbf{K}}_g^{(k)}$, matrices of the ES-DSG3 element are given by

$$\begin{aligned}\tilde{\mathbf{K}}^{(k)} &= \int_{\Omega^{(k)}} (\tilde{\mathbf{B}}^b)^T \mathbf{D}^b \tilde{\mathbf{B}}^b d\Omega + \int_{\Omega^{(k)}} (\tilde{\mathbf{B}}^s)^T \bar{\mathbf{D}}^s \tilde{\mathbf{B}}^s d\Omega \\ &= (\tilde{\mathbf{B}}^b)^T \mathbf{D}^b \tilde{\mathbf{B}}^b A^{(k)} + (\tilde{\mathbf{B}}^s)^T \bar{\mathbf{D}}^s \tilde{\mathbf{B}}^s A^{(k)},\end{aligned} \tag{42}$$

$$\tilde{\mathbf{K}}_g^{(k)} = \int_{\Omega^{(k)}} \tilde{\mathbf{B}}^{gT} \boldsymbol{\tau}\, \tilde{\mathbf{B}}^g d\Omega = \tilde{\mathbf{B}}^{gT} \boldsymbol{\tau}\, \tilde{\mathbf{B}}^g A^{(k)}. \tag{43}$$

It can be seen from Eqs. (42) and (43) that the stiffness matrices are analytically computed from the integrated constant matrices. Note that the rank of the ES-DSG3 element is similar to that of the DSG3 element and the stability of the ES-DSG3 element is also ensured. In addition, it is found from numerical experiments of the present

Table 3
A non-dimensional frequency parameter ϖ of a CCCC plate ($a/b = 1$).

t/a	Elements	Mode sequence number					
		1	2	3	4	5	6
0.005	DSG3	8.4197	12.7720	14.9652	17.2579	21.3890	21.7600
		6.7161	9.7867	10.5673	12.9981	14.5306	15.3143
		6.1786	8.8759	9.0680	11.2452	12.2182	12.2992
		6.0889	8.7239	8.8202	10.8567	11.8519	11.8845
	ES-DSG3	6.9741	10.1934	11.4756	13.0548	15.4035	15.9360
		6.1982	9.0117	9.2894	11.5616	12.7950	13.0357
		6.0355	8.6535	8.7081	10.6584	11.7430	11.7720
		6.0158	8.6075	8.6353	10.5252	11.6032	11.6293
	Exact [69]	5.999	8.568	8.568	10.407	11.472	11.498
0.1	DSG3	6.8748	9.8938	11.0847	12.6362	15.1032	15.6402
		5.9547	8.3618	8.6293	10.2985	11.3415	11.5397
		5.7616	7.9935	8.0525	9.5772	10.4153	10.4697
		5.7337	7.9381	7.9686	9.4589	10.2758	10.3246
	ES-DSG3	6.2662	8.7952	9.6625	10.9112	12.6101	13.1360
		5.8068	8.0861	8.2701	9.8397	10.7600	10.8960
		5.7250	7.9211	7.9627	9.4499	10.2631	10.3126
		5.7141	7.8990	7.9206	9.3896	10.1935	10.2411
	Exact [69]	5.71	7.88	7.88	9.33	10.13	10.18

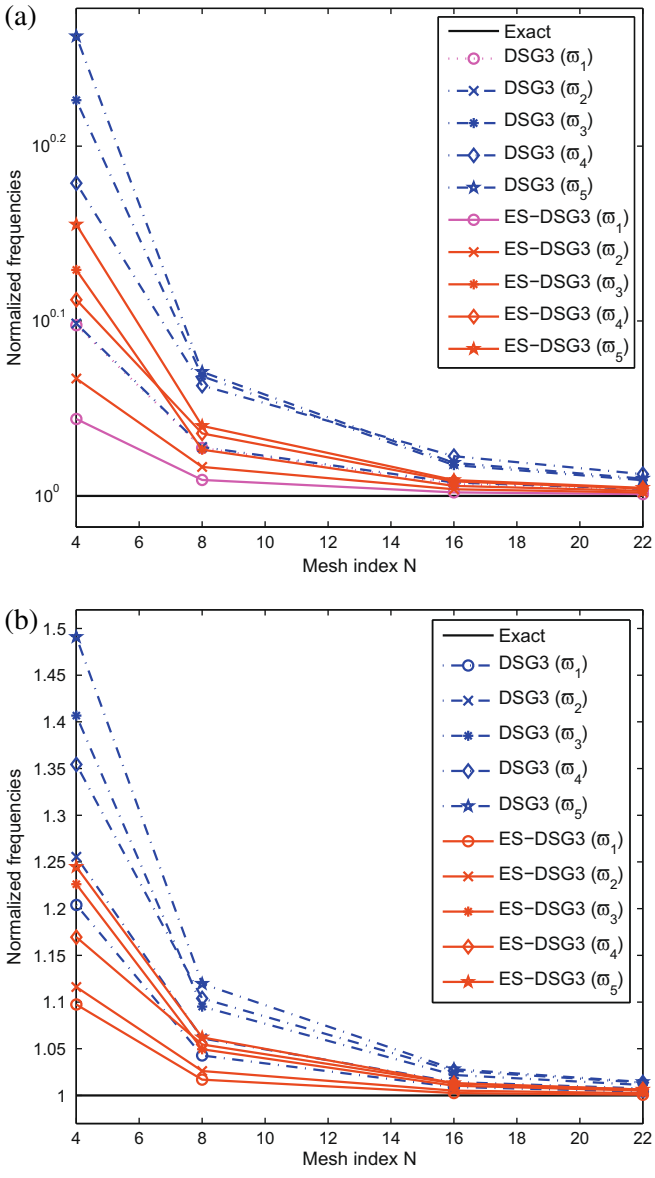

Fig. 14. Convergence of normalized frequency $\bar{\omega}^h/\bar{\omega}_{\text{exact}}$ with $a/b = 1$; $t/a = 0.005$: (a) SSSS plate; (b) CCCC plate.

formulation that the stabilized parameter α fixed at 0.05 for static problems and 0.1 for dynamics problems can produce the reasonable accuracy for all cases tested. Related to the influence of α on the accuracy of the solution, the stiffness matrix of ES-DSG3 becomes too flexible, if α is chosen too large; and the accuracy of the solution will reduce due to the oscillation of shear forces, if α is chosen too small. So far, how to obtain an "optimal" value of parameter α is still an open question.

5. Numerical results

The present element formulation has been coded using Matlab program. For practical applications, we define rotations θ_x, θ_y about the corresponding axes. Hence, the relations $\theta_x = -\beta_y$ and $\theta_y = \beta_x$ have been used to establish the stiffness formulations, see Fig. 1. For comparison, several other elements such as DSG3, MIN3 [30] and MITC4 have also been implemented in our package.

5.1. Static analysis

5.1.1. Constant bending patch test

The patch test is introduced to examine the convergence of finite elements. It is checked if the element is able to reproduce a constant distribution of all quantities for arbitrary meshes. It is modeled by several triangular elements as shown in Fig. 4. The boundary deflection is assumed to be $w = (1 + x + 2y + x^2 + -xy + y^2)/2$. The results shown in Table 1 confirm that, similar to DSG3 and MIN3 elements, the ES-DSG3 element fulfills the patch test within machine precision.

5.1.2. Square plates

Fig. 5 describes the model of a square plate (length L, thickness t) with clamped and simply supported boundary conditions, respectively, subjected to a uniform load $p = 1$. The material parameters are given by Young's modulus $E = 1{,}092{,}000$ and Poisson's ratio $\nu = 0.3$. Uniform meshes $N \times N$ with $N = 2, 4, 8, 16, 32$ are used and symmetry conditions are exploited.

For a clamped plate, the convergence of the normalized deflection and the normalized moment at the center against the mesh density N is shown in Fig. 6. The present element is free of shear locking when the plate thickness becomes small and convergent to exact solution when the mesh used is fine. It is seen that the ES-DSG3 achieves the higher accuracy compared to the DSG3 and MIN3 [30] elements. For very coarse meshes, the 4-node MITC4

Table 4
A non-dimensional frequency parameter $\varpi = \omega a^2\sqrt{\rho t/D}$ of square plate ($t/a = 0.005$) with various boundary conditions.

Plate type	Elements	Mode sequence number			
		1	2	3	4
SSSF	DSG3	11.7720	28.3759	41.9628	61.5092
	ES-DSG3	11.6831	27.8382	41.4312	59.6720
	Exact [3]	11.685	27.756	41.197	59.066
SFSF	DSG3	9.6673	16.3522	37.6792	39.5026
	ES-DSG3	9.6425	16.1239	36.9054	39.2167
	Exact [3]	9.631	16.135	36.726	38.945
CCCF	DSG3	24.2848	41.7698	65.0068	80.9461
	ES-DSG3	23.8947	40.1998	63.5127	77.8776
	Exact [3]	24.020	40.039	63.493	76.761
CFCF	DSG3	22.3437	27.1814	45.8829	62.5225
	ES-DSG3	22.1715	26.4259	43.9273	62.9466
	Exact [3]	22.272	26.529	43.664	64.466
CFSF	DSG3	15.2788	21.0199	41.1975	50.3328
	ES-DSG3	15.2035	20.5856	39.9697	49.7767
	Exact [3]	15.285	20.673	39.882	49.500

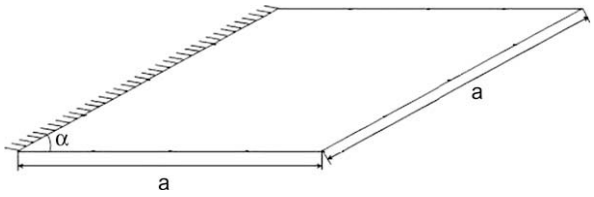

Fig. 15. The cantilever CFFF skew plate.

plate element [33] is more accurate than the ES-DSG3 element. However, the ES-DSG3 element becomes more accurate than the MITC4 element for finer meshes. Fig. 7 plots the convergence rate in energy error norm for a relation $t/L = 0.001$. It is found that the present element gains the highest accuracy in energy for this case.

For a simply supported plate, Fig. 8 illustrates the convergence of the normalized deflection and the normalized moment at the center and the convergence rate in energy error norm with a relation $t/L = 0.01$ is given in Fig. 9. It is clear that the ES-DSG3 element is still superior to the DSG3 and MIN3 elements. For the convergence of the central deflection, the MITC4 element is the most effective. For the convergence of moment and energy with fine meshes, the ES-DSG3 element is slightly more accurate than the MITC4 element.

Now we mention the computational efficiency of present method compared with FEM models. The program is compiled by a personal computer with Intel(R) Core (TM) 2 Duo CPU-2 GHz and RAM-2GB. The computational cost is to set up the global stiffness matrix and to solve the algebraic equations. Owing to the establishment of the smoothed strains (36), no additional degrees of freedom are needed in the ES-DSG3. Fig. 10 illustrates

Table 5
A non-dimensional frequency parameter $\varpi = (\omega a^2/\pi^2)\sqrt{\rho t/D}$ of a CFFF rhombic plate.

t/a	Elements	Mode sequence number					
		1	2	3	4	5	6
0.001	DSG3	0.3988	0.9580	2.5996	2.6562	4.2551	5.2267
	ES-DSG3	0.3976	0.9532	2.5785	2.6400	4.2209	5.1825
	Ref. [70]	0.398	0.954	2.564	2.627	4.189	5.131
0.2	DSG3	0.3785	0.8262	2.0109	2.1918	3.1631	3.8302
	ES-DSG3	0.3772	0.8192	1.9933	2.1785	3.1296	3.7937
	Ref. [70]	0.377	0.817	1.981	2.166	3.104	3.760

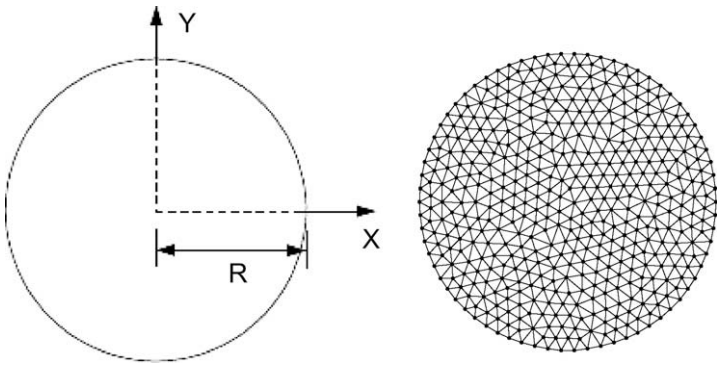

Fig. 16. The circle plates and initial mesh.

Table 6
The parameterized natural frequencies $\varpi = (\omega R^2)\sqrt{\rho t/D}$ of a clamped circular plate with $t/(2R) = 0.01$.

Mode	DSG3	ES-DSG3	ANS4 [72]	ANS9 [73]	Exact [3]	Exact [71]
1	10.2941	10.2402	10.2572	10.2129	10.2158	10.216
2	21.6504	21.3966	21.4981	21.2311	21.2600	21.260
3	21.6599	21.4096	21.4981	21.2311	21.2600	21.260
4	35.9885	35.3012	35.3941	34.7816	34.8800	34.877
5	35.9981	35.3277	35.5173	34.7915	34.8800	34.877
6	41.1864	40.3671	40.8975	39.6766	39.7710	39.771
7	53.4374	52.0138	52.2054	50.8348	51.0400	51.030
8	53.5173	52.1013	52.2054	50.8348	51.0400	51.030
9	64.2317	62.3053	63.2397	60.6761	60.8200	60.829
10	64.4073	62.4665	63.2397	60.6761	60.8200	60.829
11	74.2254	71.6554	71.7426	69.3028	69.6659	69.666
12	74.3270	71.7269	72.0375	69.3379	69.6659	69.666
13	91.4366	87.7019	88.1498	84.2999	84.5800	84.583
14	91.5328	87.7861	89.3007	84.3835	84.5800	84.583

Table 7
The parameterized natural frequencies $\varpi = (\omega R^2)\sqrt{\rho t/D}$ of a clamped circular plate with $t/(2R) = 0.1$.

Mode	DSG3	ES-DSG3	Exact [71]	ANS4 [72]^1	ANS4 [72]^2
1	9.3012	9.2527	9.240	9.2605	9.2277
2	18.0038	17.8372	17.834	17.9469	17.8010
3	18.0098	17.8428	17.834	17.9469	17.8010
4	27.6010	27.2344	27.214	27.0345	26.6801
5	27.6082	27.2391	27.214	27.6566	27.2246
6	30.9865	30.5173	30.211	30.3221	29.8562
7	37.9464	37.2817	37.109	37.2579	36.3966
8	37.9817	37.3128	37.109	37.2579	36.3966
9	43.9528	43.0626	42.409	43.2702	42.1089
10	44.0324	43.1328	42.409	43.2702	42.1089
11	48.9624	47.8823	47.340	47.7074	46.0596
12	48.9793	47.8976	47.340	47.8028	46.0985
13	57.2487	55.7747	54.557	56.0625	53.9332
14	57.2776	55.8052	54.557	57.1311	54.7720

Note: The alternative form of MITC4 [72]^1 using a consistent mass; the alternative form of MITC4 [72]^2 using a lumped mass.

the error in energy norm against the CPU time (s) for clamped plate. It is observed that the "over-head" computational cost of the ES-DSG3 is little larger than those of the MIN3, DSG3 and MITC4, due to the additional time by the smoothing operations related to the stiffness matrix. However, in terms of the computational efficiency (computation time for the same accuracy) measured in the error of energy norm, the ES-DSG3 is clearly more effective, compared to all these methods as illustrated in Fig. 10.

5.1.3. Skew plate subjected to a uniform load

Let us consider a rhombic plate subjected to a uniform load $p = 1$ as shown in Fig. 11. This plate was originally studied by Morley [66]. Dimensions and boundary conditions are specified in Fig. 11, too. Geometry and material parameters are length $L = 100$, thickness $t = 0.1$, Young's modulus $E = 10.92$ and Poisson's ratio $\nu = 0.3$.

The values of the deflection and principle moments at the central point of the ES-DSG3 in comparison with those of other methods are given in Fig. 12. It is seen again that the ES-DSG3 element shows remarkably excellent performance compared to the DSG3, MITC4 elements and the list of other elements found in [67].

5.2. Free vibration of plates

In this section, we investigate the accuracy and efficiency of the ES-DSG3 element for analyzing natural frequencies of plates. The plate may have free (F), simply (S) supported or clamped (C) edges. The symbol, CFSF, for instance, represents clamped, free, supported and free boundary conditions along the edges of rectangular plate. A non-dimensional frequency parameter ϖ is often used to stand for the frequencies and the obtained results use the regular meshes. The results of the present method are then compared to analytical solutions and other numerical results which are available in the literature.

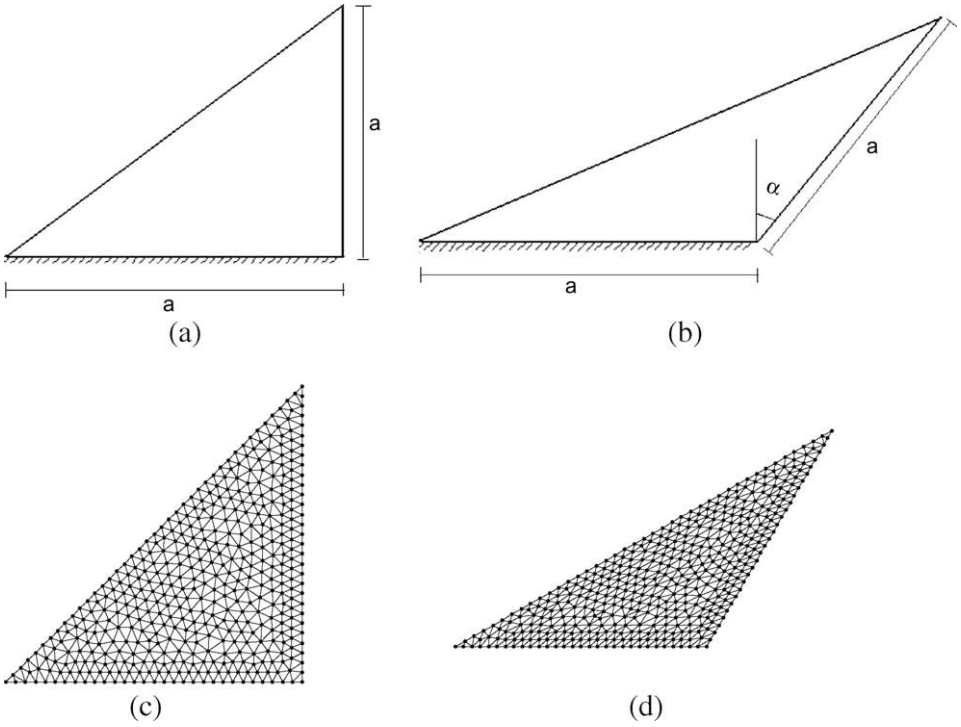

Fig. 17. A triangular cantilever plates and mesh of it: (a) square triangular plate, (b) rhombic triangular plate, (c,d) its mesh grid.

Table 8
The parameterized natural frequencies $\varpi = (\omega a^2/\pi^2)\sqrt{\rho t/D}$ of triangular plates with $t/a = 0.001$.

α^0	Elements	Mode sequence number					
		1	2	3	4	5	6
0	DSG3	0.6252	2.3890	3.3404	5.7589	7.8723	10.3026
	ES-DSG3	0.6242	2.3789	3.3159	5.7124	7.7919	10.1547
	Rayleigh–Ritz [74]	0.624	2.377	3.308	5.689	7.743	–
	Pb2 Rayleigh–Ritz [75]	0.625	2.377	3.310	5.689	7.743	–
	Experimental [76]	0.588	2.318	3.239	5.540	7.518	–
	ANS4 [72]	0.624	2.379	3.317	5.724	7.794	10.200
15	DSG3	0.5855	2.1926	3.4528	5.3481	7.3996	10.2498
	ES-DSG3	0.5840	2.1833	3.4163	5.3020	7.3112	10.0779
	Rayleigh–Ritz [74]	0.584	2.181	3.409	5.280	7.264	–
	Pb2 Rayleigh–Ritz [75]	0.586	2.182	3.412	5.279	7.263	–
	ANS4 [72]	0.583	2.181	3.413	5.303	7.289	10.095
30	DSG3	0.5798	2.1880	3.7157	5.5983	7.2814	10.7753
	ES-DSG3	0.5766	2.1778	3.6539	5.5361	7.1628	10.5108
	Rayleigh–Ritz [74]	0.576	2.174	3.639	5.511	7.108	–
	Pb2 Rayleigh–Ritz [75]	0.578	2.178	3.657	5.518	7.109	–
	ANS4 [72]	0.575	2.174	3.638	5.534	7.139	10.477
45	DSG3	0.6006	2.3564	4.2795	6.5930	7.8615	11.7850
	ES-DSG3	0.5923	2.3359	4.1699	6.4424	7.6658	11.3496
	Rayleigh–Ritz [74]	0.590	2.329	4.137	6.381	7.602	–
	Pb2 Rayleigh–Ritz [75]	0.593	2.335	4.222	6.487	7.609	–
	ANS4 [72]	0.588	2.324	4.126	6.381	7.614	11.224
60	DSG3	0.6497	2.7022	5.6491	8.3505	10.7757	14.6003
	ES-DSG3	0.6261	2.6101	5.4283	7.7333	10.3756	13.3296
	Rayleigh–Ritz [74]	0.617	2.576	5.376	7.524	10.285	–
	Pb2 Rayleigh–Ritz [75]	0.636	2.618	5.521	8.254	10.395	–
	ANS4 [72]	0.613	2.564	5.353	7.460	10.306	12.942

5.2.1. Square plates

We consider square plates of length a, width b and thickness t. The material parameters are Young's modulus $E = 2.0 \times 10^{11}$, Poisson's ratio $\nu = 0.3$ and the density mass ρ=8000. The plate is modeled with uniform meshes of 4, 8, 16 and 22 elements per each side. A non-dimensional frequency parameter $\varpi = (\omega^2 \rho a^4 t/D)^{1/4}$ is used, where $D = Et^3/(12(1-\nu^2))$ is the flexural rigidity of the plate.

The first problem considered is a SSSS thin and thick plate corresponding to length-to-width ratios, $a/b = 1$ and thickness-to-length $t/a = 0.005$ and $t/a = 0.1$. The geometry of the plate and its mesh grid are shown in Fig. 13a and c-d, respectively. Table 2 gives the convergence of six lowest frequencies corresponding to meshes using 4×4, 8×8, 16×16 and 22×22 rectangular elements. It is observed that the results of ES-DSG3 agree well with the analytical results [68] and are more accurate than those of the DSG3 element for both thin and thick plates.

The second problem is a CCCC square plate shown in Fig. 13b. Meshes are obtained the same as the SSSS plate case. Table 3 shows the convergence of eight lowest modes of a CCCC plate. It is found again that the ES-DSG3 element is better than the DSG3 element. Fig. 14 also illustrates clearly the convergence of computed frequencies ($\varpi^h/\varpi_{\text{exact}}$) of SSSS and CCCC plates.

We further study the five sets of various boundary conditions in this example: SSSF, SFSF, CCCF, CFCF, CFSF. In this case, a 20×20 regular mesh is utilized for a square plate with various boundary conditions and the first four lowest frequencies are presented in Table 4. As a result, the ES-DSG3 element is almost better than the DSG3 element and gives a good agreement with the exact solution [3] for all frequencies examined in this problem.

5.2.2. The parallelogram plates

Let us consider the thin and thick cantilever rhombic (CFFF) plates. The geometry of the plate is illustrated in Fig. 15a with skew angle $\alpha = 60^0$. The material parameters are Young's modulus $E = 2.0 \times 10^{11}$, Poisson's ratio $\nu = 0.3$ and the density mass ρ = 8000. A non-dimensional frequency parameter ϖ is used. The total number of DOF used to analyze the convergence of modes is 1323 dofs. Table 5 shows the convergence of six lowest frequencies of a CFFF rhombic plate. The solution of the ES-DSG3 element is often found closer to that of the semi-analytical method using the pb-2 Ritz method [70] than that of the DSG3 element.

5.2.3. Circle plates

In this example, a circular plate with the clamped boundary is studied as shown in Fig. 16. The material parameters are Young's modulus $E = 2.0 \times 10^{11}$, Poisson's ratio $\nu = 0.3$, the radius $R = 5$ and the density mass $\rho = 8000$. The plate is discretized into 848 triangular elements with 460 nodes. Two thickness-span ratios $h/(2R) = 0.01$ and 0.1 are considered. As shown in Table 6, the frequencies obtained from the ES-DSG3 element are closer to analytical solutions in Refs. [3,71] than that of the DSG3 element and is a good competitor to quadrilateral plate elements such as the Assumed Natural Strain solutions (ANS4) [72] and the higher order Assumed Natural Strain solutions (ANS9) [73]. In case of the thickness-span ratio $h/(2R) = 0.1$, the ES-DSG3 results also are very good in comparison to the ANS4 element that used 432 quadrilateral elements (or 864 triangular elements), cf. Table 7.

5.2.4. Triangular plates

Let us consider cantilever (CFF) triangular plates with various shape geometries, see Fig. 17a and b. The material parameters are Young's modulus $E = 2.0 \times 10^{11}$, Poisson's ratio $\nu = 0.3$ and the density mass $\rho = 8000$. A non-dimensional frequency parameter $\varpi = \omega a^2(\rho\ \mathrm{t/D})^{1/2}/\pi^2$ of triangular square plates with the aspect ratio $t/a = 0.001$ and 0.2 are calculated. The mesh of 744 triangular elements with 423 nodes is used to analyze the convergence for modes via various skew angles such as $\alpha = 0, 15, 30, 45, 60$. Table 8 gives the convergence of six lowest modes of the thin triangular plate ($t/a = 0.001$). In addition, the convergence of the frequencies is also illustrated in Fig. 18. The ES-DSG3 element is also compared to the alternative MITC4 finite element formulation [72] (the As-

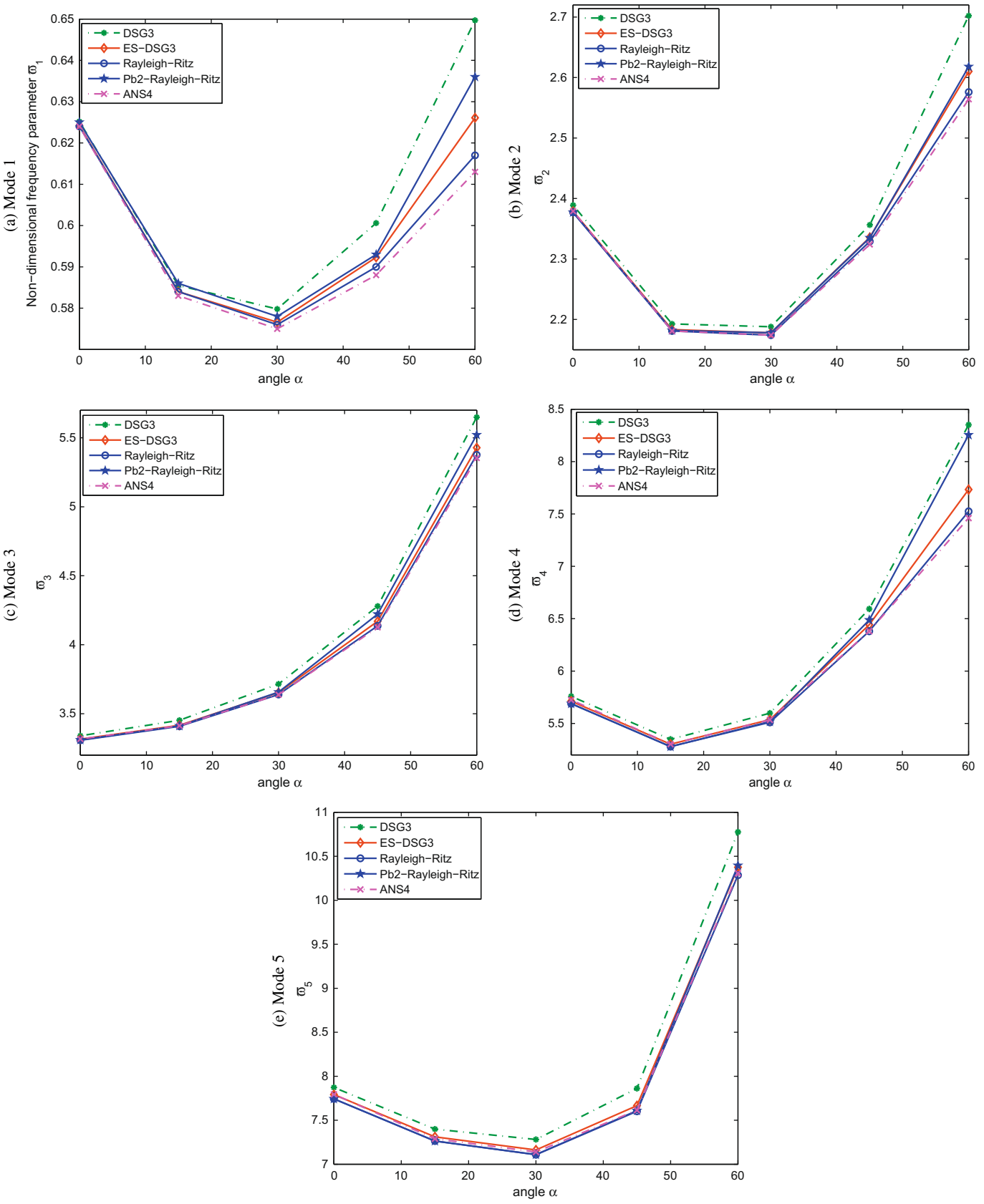

Fig. 18. Variation of the first five frequencies of triangular plate with angle α ($t/a = 0.001$).

sumed Natural Strain method (ANS4) using a mesh of 398 4-node quadrilateral elements or 796 triangular elements) and two other well-known numerical methods such as the Rayleigh–Ritz method [74] and the pb-2 Ritz method [75]. From the results given in Table 8 and Fig. 18, it is observed that the frequencies of the ES-DSG3 are often bounded by the solutions of the Rayleigh–Ritz

Table 9
The parameterized natural frequencies $\varpi = (\omega a^2/\pi^2)\sqrt{\rho t/D}$ of triangular plates with the aspect ratio $a/b = 1$ and $t/b = 0.2$.

α^0	Elements	Mode sequence number					
		1	2	3	4	5	6
0	DSG3	0.5830	1.9101	2.4176	3.9772	5.0265	5.9521
	ES-DSG3	0.5823	1.9040	2.4083	3.9559	4.9954	5.8994
	Pb2 Rayleigh–Ritz [75]	0.582	1.900	2.408	3.936	–	–
	FEM [77]	0.581	1.901	2.410	–	–	–
	ANS4 [72]	0.582	1.915	2.428	3.984	5.018	5.944
15	DSG3	0.5449	1.7803	2.3959	3.6668	4.8504	5.6057
	ES-DSG3	0.5441	1.7749	2.3854	3.6467	4.8208	5.5385
	Pb2 Rayleigh–Ritz [75]	0.544	1.771	2.386	3.628	–	–
	FEM [77]	0.543	1.770	2.388	–	–	–
	ANS4 [72]	0.545	1.764	2.420	3.608	4.820	5.431
30	DSG3	0.5339	1.7815	2.4356	3.6085	4.7829	5.4532
	ES-DSG3	0.5328	1.7754	2.4206	3.5842	4.7444	5.3377
	Pb2 Rayleigh–Ritz [75]	0.533	1.772	2.419	3.565	–	–
	FEM [77]	0.532	1.769	2.419	–	–	–
	ANS4 [72]	0.532	1.773	2.437	3.591	4.765	5.323
45	DSG3	0.5412	1.8977	2.5304	3.7518	4.8188	5.4304
	ES-DSG3	0.5391	1.8882	2.5004	3.7035	4.6800	5.2256
	Pb2 Rayleigh–Ritz [75]	0.540	1.885	2.489	3.674	–	–
	FEM [77]	0.538	1.881	2.482	–	–	–
	ANS4 [72]	0.541	1.884	2.518	3.748	4.740	5.292
60	DSG3	0.5634	2.0837	2.5355	4.0862	4.6612	5.9782
	ES-DSG3	0.5588	2.0623	2.4356	3.8009	4.3393	5.5835
	Pb2 Rayleigh–Ritz [75]	0.559	2.059	2.396	3.590	–	–
	FEM [77]	0.555	2.047	2.386	–	–	–
	ANS4 [72]	0.559	2.095	2.483	3.910	4.517	5.763

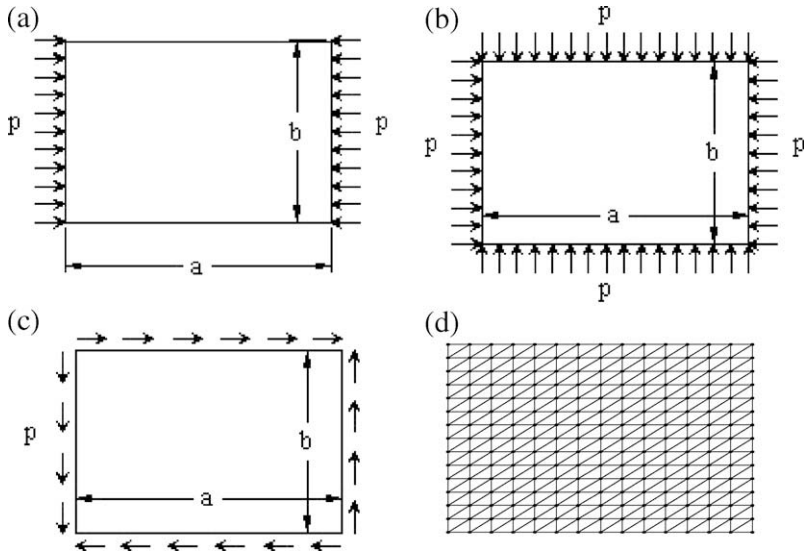

Fig. 19. Rectangular plates: (a) Axial compression, (b) biaxial compression, (c) shear in-plane, (d) regular mesh.

Table 10
The factors K of axial buckling loads along the x axis of rectangular plates with length-to-width ratios $a/b = 1$ and thickness-to-width ratios $t/b = 0.01$.

Plates type	Elements	4×4	8×8	12×12	16×16	20×20
SSSS	DSG3	7.5891	4.8013	4.3200	4.1590	4.0889
	ES-DSG3	4.7023	4.1060	4.0368	4.0170	4.0089
CCCC	DSG3	31.8770	14.7592	11.9823	11.0446	10.6282
	ES-DSG3	14.7104	11.0428	10.3881	10.2106	10.1410

and the pb-2 Ritz models. Note that our method is simply based on the formulation of 3-node triangular elements without adding any additional DOFs. Therefore, the ES-DSG3 is very promising to provide an effective tool together with existing numerical models. Also, Table 9 again shows that the ES-DSG3 works well for this thick plate problem.

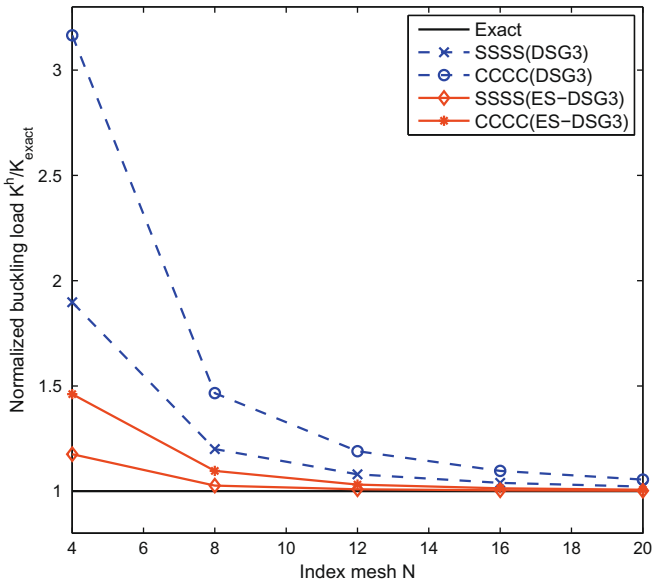

Fig. 20. The convergence of buckling load K^h of square plate with $t/b = 0.01$.

5.3. Buckling of plates

In the following examples, the factor of buckling load is defined as $K = \lambda_{cr} b^2/(\pi^2 D)$ where b is the edge width of the plate, λ_{cr} the critical buckling load. The material parameters are Young's modulus $E = 2.0 \times 10^{11}$, Poisson's ratio v=0.3.

5.3.1. Simply supported rectangular plates subjected to uniaxial compression

Let us first consider a plate with length a, width b and thickness t subjected to a uniaxial compression. Simply supported (SSSS) and clamped (CCCC) boundary conditions are assumed. The geometry and regular mesh of the plate are shown in Fig. 19a and d, respectively. Table 10 gives the convergence of the buckling load factor corresponding to the meshes of 4×4, 8×8, 12×12, 16×16 and 20×20 rectangular elements. Fig. 20 plots the convergence of the normalized buckling load K^h/K_{exact} of square plate with the thickness ratio $t/b = 0.01$, where K^h, K_{exact} are the buckling load of numerical methods and the buckling load of the analytical solution [78], respectively. It is evident that the ES-DSG3 element converges to the exact solution faster than the DSG3 element. In addition, the performance of the ES-DSG3 element is also compared with several

Table 13
The factor K^h of axial buckling loads along the x axis of rectangular plates with various length-to-width ratios and various thickness-to-width ratios.

a/b	t/b	DSG3	ES-DSG3	Meshfree [8]	Pb-2 Ritz [80]
0.5	0.05	6.0478	5.9873	6.0405	6.0372
	0.1	5.3555	5.3064	5.3116	5.4777
	0.2	3.7524	3.7200	3.7157	3.9963
1.0	0.05	3.9786	3.9412	3.9293	3.9444
	0.1	3.7692	3.7402	3.7270	3.7865
	0.2	3.1493	3.1263	3.1471	3.2637
1.5	0.05	4.3930	4.2852	4.2116	4.2570
	0.1	4.0604	3.9844	3.8982	4.0250
	0.2	3.2014	3.1461	3.1032	3.3048
2.0	0.05	4.1070	3.9811	3.8657	3.9444
	0.1	3.8539	3.7711	3.6797	3.7865
	0.2	3.2023	3.1415	3.0783	3.2637
2.5	0.05	4.3577	4.1691	3.9600	4.0645
	0.1	4.0644	3.8924	3.7311	3.8683
	0.2	3.2393	3.1234	3.0306	3.2421

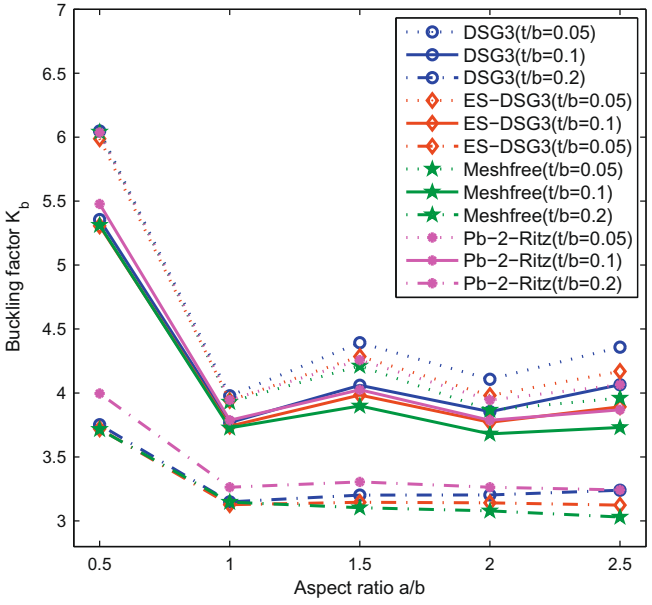

Fig. 21. Variation of axial buckling load K_b of SSSS plate with various length-to-width ratios and various thickness-to-width ratios.

Table 11
The factor K_b of axial buckling loads along the x axis of rectangular plates with length-to-width ratios $a/b = 1$ and thickness-to-width ratios $t/b = 0.01$.

Plate types	DSG3	ES-DSG3	Liew and Chen [79]	Ansys [79]	Timoshenko and Gere [78]	Tham and Szeto [82]	Vrcelj and Bradford [83]
SSSS	4.1590	4.0170	3.9700	4.0634	4.00	4.00	4.0006
	(3.97%)	(0.4%)	(−0.75%)	(1.85%)	(0.0%)	(0.0%)	(0.02%)
CCCC	11.0446	10.2106	10.1501	10.1889	10.07	10.08	10.0871
	(9.68%)	(1.4%)	(0.8%)	(1.18%)	(0.0%)	(0.1%)	(0.17%)

Table 12
The factor K^h of axial buckling loads along the x axis of rectangular plates with various length-to-width ratios $a/b = 1$ and various thickness-to-width ratios.

t/b	Plate types	DSG3	ES-DSG3	RPIM [79]	Pb-2 Ritz [80]
0.05	SSSS	3.9786	3.9412	3.9464	3.9444
	CCCC	9.8284	9.5426	9.5819	9.5586
	FCFC	3.8365	3.7654	3.8187	3.8005
0.1	SSSS	3.7692	3.7702	3.7853	3.7873
	CCCC	8.2670	8.2674	8.2931	8.2921
	FCFC	3.4594	3.4966	3.5138	3.5077

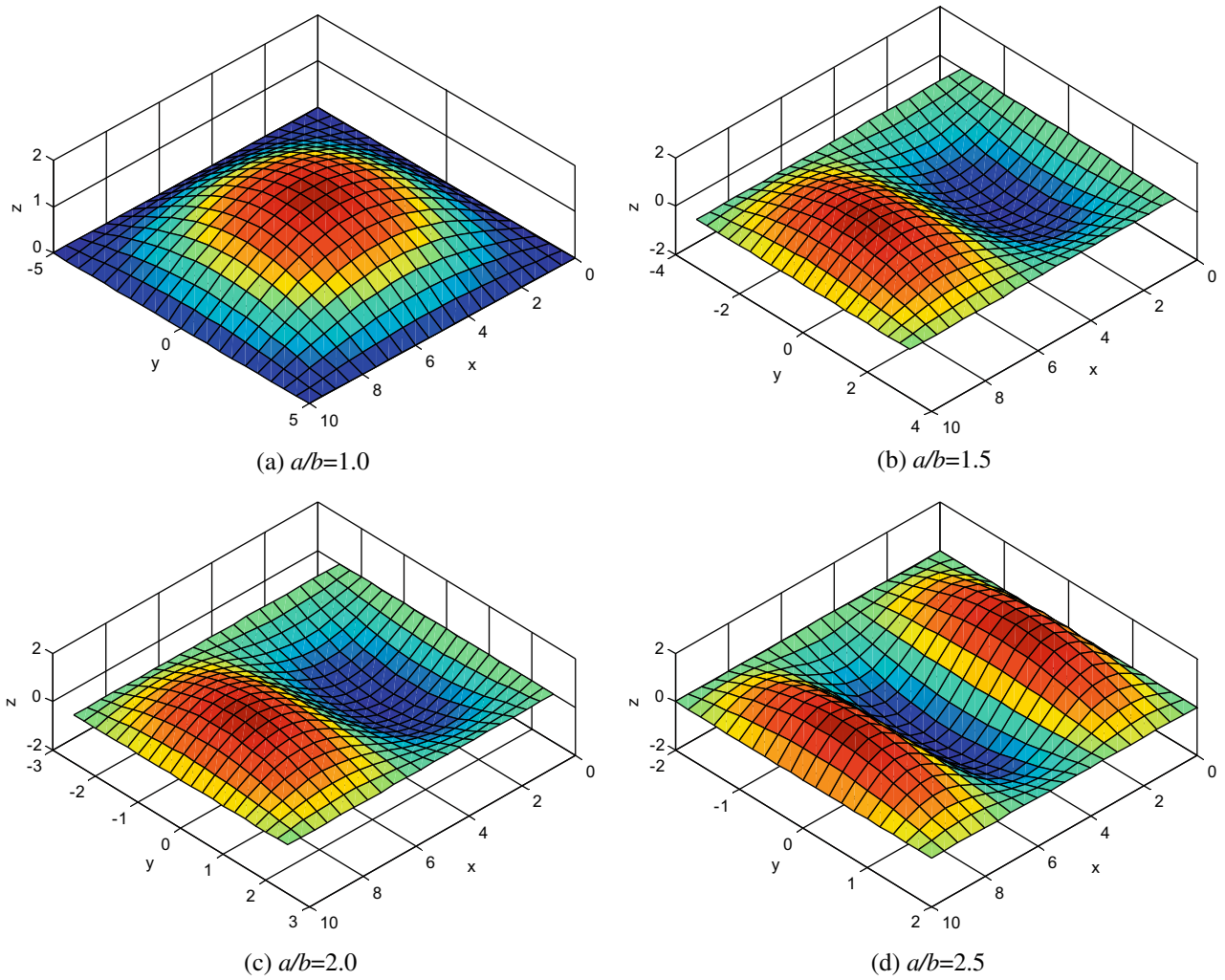

Fig. 22. Axial buckling modes of simply-supported rectangular plates with thickness-to-width ratios $t/b = 0.01$ and various length-to-width ratios (a) $a/b = 1.0$; (b) $a/b = 1.5$; (c) $a/b = 2.0$; (d) $a/b = 2.5$.

Table 14
The factors K^h of biaxial buckling loads of rectangular plates with length-to-width ratios $a/b = 1$, thickness-to-width ratios $t/b = 0.01$ and various boundary conditions.

Plates type	DSG3	ES-DSG3	Timoshenko and Gere [78]	Tham and Szeto [82]	Vrcelj and Bradford [83]
SSSS	2.0549	2.0023	2.00	2.00	2.0008
CCCC	5.6419	5.3200	5.31	5.61	5.3260
SCSC	4.0108	3.8332	3.83	3.83	3.8419

other methods in the literature. Table 11 shows the factor values K^h using $2 \times 16 \times 16$ triangular elements, and the relative error percentages compared with exact results are given in parentheses. It is found that the ES-DSG3 results agree well with analytical solution [78], spline finite strip methods [82,83] and the radial point interpolation meshfree method [79].

Next we consider the buckling load factors of SSSS, CCCC, FCFC plate with thickness-to-width ratios $t/b = 0.05; 0.1$. The results are given in Table 12. The present results are compared with the radial point interpolation meshfree method [79], the pb-2 Ritz method [80] and a good agreement is found.

More details, we also consider simply supported plates with various thickness-to-width ratios, $t/b = 0.05; 0.1; 0.2$ and length-to-width ratios, $a/b = 0.5; 1.0; 1.5; 2.0; 2.5$. Table 13 and Fig. 21 show the buckling factors using the regular mesh of 16×16 rectangular elements. The DSG3 and ES-DSG3 results are also compared to the pb-2 Ritz and meshfree method [8]. It is seen that the ES-DSG3 exhibits a good agreement with meshfree method and the pb-2 Ritz method [80]. Fig. 22 also depicts the axial buckling modes of simply-supported rectangular plates with thickness-to-width ratios $t/b = 0.01$ and various length-to-width ratios, $a/b = 1.0; 1.5; 2.0; 2.5$.

Table 15
The factors K^h of shear buckling loads of simply supported rectangular plates with various length-to-width ratios, choose $t/b = 0.01$.

a/b	DSG3	ES-DSG3	Meshfree [8]	Exact [81]
1.0	9.5195	9.2830	9.3962	9.34
2.0	6.7523	6.4455	6.3741	6.34
3.0	6.5129	5.8830	5.7232	5.784
4.0	6.3093	5.6732	5.4367	5.59

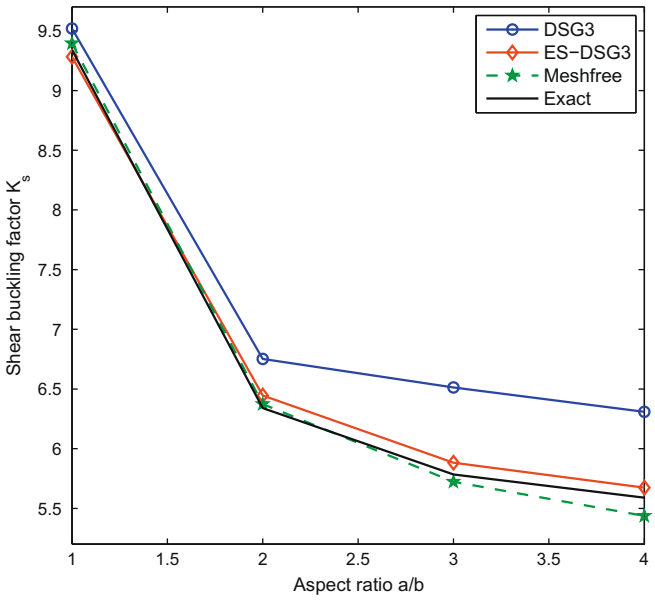

Fig. 23. Variation of shear buckling load of simply-supported rectangular plates with various length-to-width ratios.

5.3.2. Simply supported rectangular plates subjected to biaxial compression

The square plate subjected to biaxial compression is considered. The geometry of the plates is shown in Fig. 19b. Table 14 gives the shear buckling factor of square plate subjected biaxial compression with three essential boundary conditions (SSSS, CCCC, SCSC) using $2 \times 16 \times 16$ triangular elements. It can be seen that the ES-DSG3 element matches well with the analytical solution [78] and the spline finite strip methods [82,83].

5.3.3. Simply supported rectangular plates subjected to in-plane pure shear

Consider the simply supported plate subjected to in-plane shear shown in Fig. 19c. The factors K^h of shear buckling loads of this plate are calculated using 16×16 rectangular elements. The shear buckling factors with thickness-to-width ratio, $t/b = 0.001$ and length-to-width ratios, $a/b = 1.0$; 2.0; 3.0; 4.0 are listed in Table 15. The present results are compared to the exact solutions in [81] and the meshfree solution [8]. It can be seen that the ES-DSG3 element agrees well with the exact solution. We can be concluded that the factor of buckling load of the plate is well approximated by the present method. The convergence of the shear buckling load of a support plate is illustrated in Fig. 23. The shear buckling load decreases rapidly as length-to-width ratios increase.

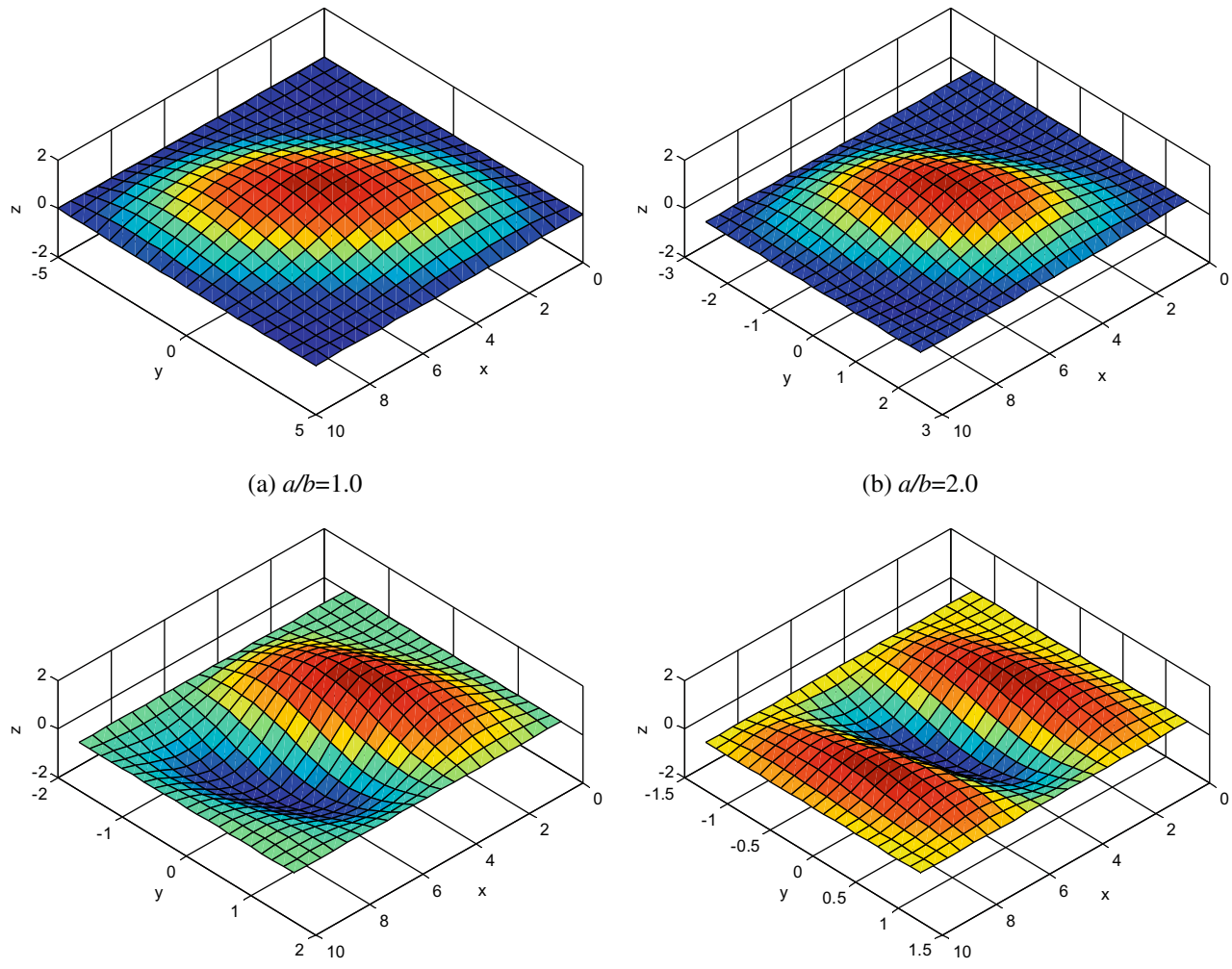

(a) a/b=1.0 (b) a/b=2.0

(c) a/b=3.0 (b) a/b=4.0

Fig. 24. Shear buckling mode of simply-supported rectangular plates using the ES-DSG3 with various length-to-width ratios; (a) $a/b = 1.0$; (b) $a/b = 2.0$; (c) $a/b = 3.0$; (d) $a/b = 4.0$.

Table 16
The factors K^h of shear buckling loads of rectangular plates with length-to-width ratios $a/b = 1$, thickness-to-width ratios $t/b = 0.01$ and various boundary condition.

Plates type	DSG3	ES-DSG3	Timoshenko and Gere [78]	Tham and Szeto [82]	Vrcelj and Bradford [83]
SSSS	9.5195	9.2830	9.33	9.40	9.3847
CCCC	15.6397	14.6591	14.66	14.58	14.6601
SCSC	13.1652	12.5533	12.58	12.58	12.5997

Fig. 24 shows the shear buckling modes of simply-supported rectangular plates with thickness-to-width ratios $t/b = 0.01$ and various length-to-width ratios, $a/b = 1.0$; 2.0; 3.0; 4.0.

Now we consider the square subjected to in-plane shear with three essential boundary conditions, SSSS, CCCC, SCSC. The present result is given in Table 16. It can be again seen that the ES-DSG3 element is very good in comparison to the analytical solution [78], the spline finite strip methods [82,83].

6. Conclusions

An edge-based smoothed finite element method with the stabilized Discrete Shear Gap technique using triangular elements is formulated for static, free vibration and buckling analyses of Reissner–Mindlin plates. Through the formulations and numerical examples, some concluding remarks can be drawn as follows:

- The ES-DSG3 uses only three DOFs at each vertex node without additional degrees of freedom and no more requirement of high computational cost.
- The ES-DSG3 element is more accurate than the DSG3, MIN3 triangular elements, and often found more accurate than the well-known MITC4 element when the same sets of nodes are used for all cases studied. The results of the ES-DSG3 element are also in a good agreement with analytical solution and compared well with results of several other published elements in the literature.
- For free vibration and buckling analyses, no spurious non-zero energy modes are observed and hence the ES-DSG3 element is stable temporally. The ES-DSG3 element gives more accurate results than the DSG3 element and shows also a strong competitor to existing complicated models such as the Rayleigh–Ritz method, the pb-2 Ritz method, the spline finite strip and the meshfree approaches.

Through the obtained results, the present method is thus very promising to provide a simple and effective tool for analyses of plate structures.

References

[1] J. Mackerle, Finite element linear and nonlinear, static and dynamic analysis of structural elements: a bibliography (1992–1995), Engrg. Comput. 14 (4) (1997) 347–440.
[2] J. Mackerle, Finite element linear and nonlinear, static and dynamic analysis of structural elements: a bibliography (1999–2002), Engrg. Comput. 19 (5) (2002) 520–594.
[3] A.W. Leissa, Vibration of Plates, NASA, SP-160, Washington DC, 1969.
[4] A.W. Leissa, Plate vibration research: 1981–1985: classical theory, Shock Vib. Dig. 19 (1987) 11–18.
[5] [22] A.W. Leissa, A review of laminated composite plate buckling, Appl. Mech. Rev. 40 (5) (1987) 575–591.
[6] A.W. Leissa, Buckling and postbuckling theory for laminated composite plates, in: G.J. Turvey, I.H. Marshall (Eds.), Buckling and Postbuckling of Composite Plates, Chapman & Hall, London, UK, 1995, pp. 1–29.
[7] K.M. Liew, Y. Xiang, S. Kitipornchai, Research on thick plate vibration: a literature survey, J. Sound Vib. 180 (1) (1995) 163–176.
[8] K.M. Liew, J. Wang, T.Y. Ng, M.J. Tan, Free vibration and buckling analyses of shear-deformable plates based on FSDT meshfree method, J. Sound Vib. 276 (2004) 997–1017.
[9] O.C. Zienkiewicz, R.L. Taylor, J.M. Too, Reduced integration technique in general analysis of plates and shells Simple and efficient element for plate bending, Int. J. Numer. Methods Engrg. 3 (1971) 275–290.
[10] T.J. R Hughes, R.L. Taylor, W. Kanoknukulchai, Simple and efficient element for plate bending, Int. J. Numer. Methods Engrg. 11 (1977) 1529–1543.
[11] T.J.R. Hughes, M. Cohen, M. Haroun, Reduced and selective integration techniques in finite element method of plates, Nucl. Engrg. Des. 46 (1978) 203–222.
[12] D.S. Malkus, T.J.R. Hughes, Mixed finite element methods-reduced and selective integration techniques: a unification of concepts, Comput. Methods Appl. Mech. Engrg. 46 (1978) 203–222.
[13] S.W. Lee, T.H. H Pian, Finite elements based upon Mindlin plate theory with particular reference to the four-node isoparametric element, AIAA J. 16 (1978) 29–34.
[14] S.W. Lee, C. Wong, Mixed formulation finite elements for Mindlin theory plate bending, Int. J. Numer. Methods Engrg. 18 (1982) 1297–1311.
[15] O.C. Zienkiewicz, D. Lefebvre, A robust triangular plate bending element of the Reissner–Mindlin type, Int. J. Numer. Methods Engrg. 26 (1988) 1169–1184.
[16] O.C. Zienkiewicz, Z. Xu, L.F. Zeng, A. Samuelsson, N.E. Wiberg, Linked interpolation for Reissner–Mindlin plate element: Part I – a simple quadrilateral, Int. J. Numer. Methods Engrg. 36 (1993) 3043–3056.
[17] R. Ayad, G. Dhatt, J.L. Batoz, A new hybrid-mixed variational approach for Reissner–Mindlin plate, the MiSP model, Int. J. Numer. Methods Engrg. 42 (1998) 1149–1179.
[18] C. Lovadina, Analysis of a mixed finite element method for the Reissner–Mindlin plate problems, Comput. Methods Appl. Mech. Engrg. 163 (1998) 71–85.
[19] R.L. Taylor, F. Auricchio, Linked interpolation for Reissner–Mindlin plate element: Part II – a simple triangle, Int. J. Numer. Methods Engrg. 36 (1993) 3043–3056.
[20] F. Auricchio, R.L. Taylor, A shear deformable plate element with an exact thin limit, Comput. Methods Appl. Mech. Engrg. 118 (1994) 393–412.
[21] F. Auricchio, R.L. Taylor, A triangular thick plate finite element with an exact thin limit, Finite Elem. Anal. Des. 19 (1995) 57–68.
[22] S. De Miranda, F. Ubertini, A simple hybrid stress element for shear deformable plates, Int. J. Numer. Methods Engrg. 65 (2006) 808–833.
[23] S. Brasile, An isostatic assumed stress triangular element for the Reissner–Mindlin plate-bending problem, Int. J. Numer. Methods Engrg. 74 (2008) 971–995.
[24] J.C. Simo, M.S. Rifai, A class of mixed assumed strain methods and the method of incompatible modes, Int. J. Numer. Methods Engrg. 29 (1990) 1595–1638.
[25] J.C. Simo, D.D. Fox, M.S. Rifai, On a stress resultant geometrically exact shell model. Part II: The linear theory, computational aspects, Comput. Methods Appl. Mech. Engrg. 73 (1989) 53–92.
[26] J.M.A. César de Sá, R.M. Natal Jorge, New enhanced strain elements for incompatible problems, Int. J. Numer. Methods Engrg. 44 (1999) 229–248.
[27] J.M.A. César de Sá, R.M. Natal Jorge, R.A. Fontes Valente, P.M.A. Areias, Development of shear locking-free shell elements using an enhanced assumed strain formulation, Int. J. Numer. Methods Engrg. 53 (2002) 1721–1750.
[28] R.P.R. Cardoso, J.W. Yoon, M. Mahardika, S. Choudhry, R.J. Alves de Sousa, R.A. Fontes Valente, Enhanced assumed strain (EAS) and assumed natural strain (ANS) methods for one-point quadrature solid-shell elements, Int. J. Numer. Methods Engrg. 75 (2008) 156–187.
[29] T.J. R Hughes, T. Tezduyar, Finite elements based upon Mindlin plate theory with particular reference to the four-node isoparametric element, J. Appl. Mech. 48 (1981) 587–596.
[30] A. Tessler, T.J.R. Hughes, A three-node Mindlin plate element with improved transverse shear, Comput. Methods Appl. Mech. Engrg. 50 (1985) 71–101.
[31] T.J.R. Hughes, R.L. Taylor, The linear triangular plate bending element, in: J.R. Whiteman (Ed.), The Mathematics of Finite Elements and Applications IV. MAFELAP 1981, Academic Press, 1982, pp. 127–142.
[32] R.H. MacNeal, Derivation of element stiffness matrices by assumed strain distribution, Nucl. Engrg. Des. 70 (1982) 3–12.
[33] K.J. Bathe, E.N. Dvorkin, A four-node plate bending element based on Mindlin/Reissener plate theory and a mixed interpolation, Int. J. Numer. Methods Engrg. 21 (1985) 367–383.
[34] E.N. Dvorkin, K.J. Bathe, A continuum mechanics based four-node shell element for general nonlinear analysis, Engrg. Comput. 1 (1984) 77–88.
[35] K.J. Bathe, E.N. Dvorkin, A formulation of general shell elements, the use of mixed interpolation of tensorial components, Int. J. Numer. Methods Engrg. 22 (1986) 697–722.
[36] J.L. Batoz, P. Lardeur, A discrete shear triangular nine d.o.f. element for the analysis of thick to very thin plates, Int. J. Numer. Methods Engrg. 29 (1989) 533–560.
[37] O.C. Zienkiewicz, R.L. Taylor, P. Papadopoulos, E. O~nate, Plate bending elements with discrete constraints: new triangular elements, Comput. Struct. 35 (1990) 505–522.

[38] J.L. Batoz, I. Katili, On a simple triangular Reissner/Mindlin plate element based on incompatible modes and discrete constraints, Int. J. Numer. Methods Engrg. 35 (1992) 1603–1632.
[39] K.U. Bletzinger, M. Bischoff, E. Ramm, A unified approach for shear-locking free triangular and rectangular shell finite elements, Comput. Struct. 75 (2000) 321–334.
[40] J.S. Chen, C.T. Wu, S. Yoon, Y. You, A stabilized conforming nodal integration for Galerkin mesh-free methods, Int. J. Numer. Methods Engrg. 50 (2001) 435–466.
[41] G.R. Liu, K.Y. Dai, T.T. Nguyen, A smoothed finite element for mechanics problems, Comput. Mech. 39 (2007) 859–877.
[42] G.R. Liu, T.T. Nguyen, K.Y. Dai, K.Y. Lam, Theoretical aspects of the smoothed finite element method (SFEM), Int. J. Numer. Methods Engrg. 71 (2007) 902–930.
[43] T. Nguyen-Thoi, G.R. Liu, K.Y. Dai, K.Y. Lam, Selective smoothed finite element method, Tsinghua Sci. Technol. 12 (5) (2007) 497–508.
[44] K.Y. Dai, G.R. Liu, T. Nguyen-Thoi, An n-sided polygonal smoothed finite element method (nSFEM) for solid mechanics, Finite Elem. Anal Des. 43 (2007) 847–860.
[45] K.Y. Dai, G.R. Liu, Free and forced vibration analysis using the smoothed finite element method (SFEM), J. Sound. Vib. 301 (2007) 803–820.
[46] X.Y. Cui, G.R. Liu, G.Y. Li, X. Zhao, T. Nguyen-Thoi, G.Y. Sun, A smoothed finite element method (SFEM) for linear and geometrically nonlinear analysis of plates and shells, CMES-Comput. Model. Engrg. Sci. 28 (2) (2008) 109–125.
[47] H. Nguyen-Xuan, S. Bordas, H. Nguyen-Dang, Smooth finite element methods: convergence, accuracy and properties, Int. J. Numer. Methods Engrg. 74 (2008) 175–208.
[48] H. Nguyen-Xuan, S. Bordas, H. Nguyen-Dang, Addressing volumetric locking and instabilities by selective integration in smoothed finite elements, Commun. Numer. Methods Engrg. 25 (2009) 19–34.
[49] G.R. Liu, T. Nguyen-Thoi, H. Nguyen-Xuan, K.Y. Dai, K.Y. Lam, On the essence and the evaluation of the shape functions for the smoothed finite element method (SFEM) (Letter to Editor), Int. J. Numer. Methods Engrg. 77 (2009) 1863–1869.
[50] H. Nguyen-Xuan, T. Rabczuk, S. Bordas, J.F. Debongnie, A smoothed finite element method for plate analysis, Comput. Methods Appl. Mech. Engrg. 197 (2008) 1184–1203.
[51] N. Nguyen-Thanh, T. Rabczuk, H. Nguyen-Xuan, S. Bordas, A smoothed finite element method for shell analysis, Comput. Methods Appl. Mech. Engrg. 198 (2008) 165–177.
[52] H. Nguyen-Xuan, T. Nguyen-Thoi, A stabilized smoothed finite element method for free vibration analysis of Mindlin–Reissner plates, Commun. Numer. Methods Engrg. 25 (8) (2009) 882–906.
[53] N. Moes, J. Dolbow, T. Belytschko, A finite element method for crack growth without remeshing, Int. J. Numer. Methods Engrg. 46 (1) (1999) 131–150.
[54] T. Belytschko, N. Moes, S. Usui, C. Parimi, Arbitrary discontinuities in finite elements, Int. J. Numer. Methods Engrg. 50 (2001) 993–1013.
[55] S. Bordas, P.V. Nguyen, C. Dunant, A. Guidoum, H. Nguyen-Dang, An extended finite element library, Int. J. Numer. Methods Engrg. 71 (6) (2007) 703–732.
[56] S. Bordas, T. Rabczuk, H. Nguyen-Xuan, P. Nguyen Vinh, S. Natarajan, T. Bog, Q. Do Minh, H. Nguyen Vinh, Strain smoothing in FEM and XFEM, Comput. Struct. in press, doi:10.1016/j.compstruc.2008.07.006.
[57] G.R. Liu, T. Nguyen-Thoi, H. Nguyen-Xuan, K.Y. Lam KY, A node-based smoothed finite element method (NS-FEM) for upper bound solutions to solid mechanics problems, Comput. Struct. 87 (2009) 14–26.
[58] T. Nguyen-Thoi, G.R. Liu, H. Nguyen-Xuan, C. Nguyen Tran, Adaptive analysis using the node-based smoothed finite element method (NS-FEM), Commun. Numer. Methods Engrg. (2009), doi:10.1002/cnm.1291.
[59] G.R. Liu, T. Nguyen-Thoi, K.Y. Lam, A novel alpha finite element method (α FEM) for exact solution to mechanics problems using triangular and tetrahedral elements, Comput. Methods Appl. Mech. Engrg. 197 (2008) 3883–3897.
[60] G.R. Liu, T. Nguyen-Thoi, K.Y. Lam, An edge-based smoothed finite element method (ES-FEM) for static and dynamic problems of solid mechanics, J. Sound. Vib. 320 (2008) 1100–1130.
[61] H. Nguyen-Xuan, G.R. Liu, T. Nguyen-Thoi, C. Nguyen Tran, An edge-based smoothed finite element method (ES-FEM) for analysis of two-dimensional piezoelectric structures, Smart Mater. Struct. 18 (6) (2009) 065015 (12 pp.).
[62] T. Nguyen-Thoi, G.R. Liu, H.C. Vu-Do, H. Nguyen-Xuan, An edge-based smoothed finite element method (ES-FEM) for elastoviscoplastic analyses in solid mechanics using triangular mesh, Comput. Mech. 45 (2009) 23–44.
[63] T. Nguyen-Thoi, G.R. Liu, K.Y. Lam, G.Y. Zhang, A face-based smoothed finite element method (FS-FEM) for 3D linear and nonlinear solid mechanics problems using 4-node tetrahedral elements, Int. J. Numer. Methods Engrg. 78 (2009) 324–353.
[64] Lyly M, Stenberg R, Vihinen T, A stable bilinear element for the Reissner–Mindlin plate model, Comput. Methods Appl. Mech. Engrg. 110 (1993) 343–357.
[65] M. Bischoff, K.U. Bletzinger, Stabilized DSG Plate and Shell Elements, Trends in Computational Structural Mechanics, CIMNE, Barcelona, Spain, 2001.
[66] L.S.D. Morley, Skew Plates and Structures, Pergamon Press, Oxford, 1963.
[67] S. Cen, Y.Q. Long, Z.H. Yao, S.P. Chiew, Application of the quadrilateral area co-ordinate method: a new element for Mindlin–Reissner plate, Int. J. Numer. Methods Engrg. 66 (2006) 1–45.
[68] F. Abbassian, D.J. Dawswell, N.C. Knowles, Free Vibration BenchmarksSoftback, Atkins Engineering Sciences, Glasgow, 1987. 40 p..
[69] D.B. Robert, Formulas for Natural Frequency and Mode Shape, Van Nostrand Reinhold, New York, 1979.
[70] W. Karunasena, K.M. Liew, F.G.A. Al-Bermani, Natural frequencies of thick arbitrary quadrilateral plates using the pb-2 Ritz method, J. Sound Vib. 196 (1996) 371–385.
[71] T. Irie, G. Yamada, S. Aomura, Natural frequencies of Mindlin circular plates, J. Appl. Mech. 47 (1980) 652–655.
[72] S.J. Lee, Free vibration analysis of plates by using a four-node finite element formulated with assumed natural transverse shear strain, J. Sound. Vib. 278 (2004) 657–684.
[73] S.J. Lee, S.E. Han, Free-vibration analysis of plates and shells with a nine-node assumed natural degenerated shell element, J. Sound Vib. 241 (2001) 605–633.
[74] O.G. McGee, A.W. Leissa, C.S. Huang, Vibrations of cantilevered skewed trapezoidal and triangular plates with corner stress singularities, Int. J. Mech. Sci. 34 (1992) 63–84.
[75] W. Karunasena, S. Kitipornchai, F.G.A. Al-bermani, Free vibration of cantilevered arbitrary triangular Mindlin plates, Int. J. Mech. Sci. 38 (1996) 431–442.
[76] P.N. Gustafson, W.F. Stokey, C.F. Zorowski, An experimental study of natural vibrations of cantilevered triangular plate, J. Aeronautic. Sci. 20 (1953) 331–337.
[77] O.G. McGee, T.S. Butalia, Natural vibrations of shear deformable cantilevered skewed trapezoidal and triangular thick plates, Comput. Struct. 45 (1992) 1033–1059.
[78] S.P. Timoshenko, J.M. Gere, Theory of Elastic Stability, third ed., McGraw-Hill, New York, 1970.
[79] K.M. Liew, X.L. Chen, Buckling of rectangular Mindlin plates subjected to partial in-plane edge loads using the radial point interpolation method, Int. J. Solids Struct. 41 (2004) 1677–1695.
[80] S. Kitipornchai, Y. Xiang, C.M. Wang, K.M. Liew, Buckling of thick skew plates, Int. J. Numer. Methods Engrg. 36 (1993) 1299–1310.
[81] M. Azhari, S. Hoshdar, M.A. Bradford, On the use of bubble functions in the local buckling analysis of plate structures by the spline finite strip method, Int. J. Numer. Methods Engrg. 48 (2000) 583–593.
[82] L.G. Tham, H.Y. Szeto, Buckling analysis of arbitrary shaped plates by spline finite strip method, Comput. Struct. 36 (1990) 729–735.
[83] Z. Vrcelj, M.A. Bradford, A simple method for the inclusion of external and internal supports in the spline finite strip method (SFSM) of buckling analysis, Comput. Struct. 86 (2008) 529–544.